

**THE PENMAN-MONTEITH  
SYSTEM OF EQUATIONS:  
Derivation with the  
Thermodynamic Approach,  
Numerical Solutions, and Evaluation**

D. Zerihun and C.A. Sanchez

University of Arizona  
Maricopa Agricultural Center  
37860 W. Smith-Enke Rd  
Maricopa, AZ 85138

April, 2023

## 1. Introduction

A derivation of the Penman-Monteith equation with the thermodynamic formulation of Monteith (1965,1981) is presented in this report. The resultant set of equations (consisting of expressions for latent heat flux, sensible heat flux, and the final air temperature) is shown to represent a coupled system. The report details the development and evaluation of alternative numerical solutions, based on data covering a wide range of evaporation conditions. Furthermore, equations of the resistance parameters, used to define the Penman-Monteith system of equations, are reviewed and relationships between the parameters are explored.

A review of the derivation of the Penman-Monteith equation based on the thermodynamic formulation of evaporation (Monteith, 1981) is presented in Chapter 2 of this report. Unlike the conventional approach to the derivation of the Penman-Monteith equation, where evaporation is treated as vapor and heat transfer process between two points in space (i.e., a point in the exchange surface and another one in the air current), the thermodynamic conceptualization of evaporation introduces a perspective whereby the process can be studied from the vantage point of the changes it introduces in the thermodynamic properties (specifically, the latent heat and sensible heat contents) of the ambient air.

The derivation proceeds in two steps. As an initial approximation, first a form of the equation that models evaporation into a quiescent ambient air, from a wet source/sink surface, is developed based on the thermodynamic equations of state applied to a suitably defined system. In a subsequent step, resistance parameters are introduced into the basic equations accounting for the dynamic effects of wind-surface interactions (and the effects of canopy complex response to atmospheric conditions) on evaporation, leading to the Penman-Monteith equation. Although less compact than the conventional approach (Penman, 1948; Jensen and Allen, 2016), the

thermodynamic approach to the derivation of the Penman-Monteith equation has the benefit of revealing key assumptions and concepts that are generally implicit in the conventional approach. The initial step of the thermodynamic formulation accentuates the notion that the Penman-Monteith equation is fundamentally a description of the process of vapor and heat transfer between a wet source/sink surface and a quiescent ambient air. The subsequent step, on the other hand, emphasizes the fact that wind and canopy system effects on evaporation are taken into account in an approximate sense, through the introduction of resistance parameters. While Chapter 2 essentially presents a review of the approach proposed by Monteith, the derivation here, nonetheless, emphasizes basic assumptions, clarifies concepts, and fills gaps left by the original discussion.

The derivation in Chapter 2 produces equations for latent heat flux, sensible heat flux, and the final air temperature, each expressed as a function of resistance parameters, consisting of the bulk surface resistance and the resistances to vapor and heat transfer across the turbulent boundary layer.

It is shown in Chapter 3 that under a suitably defined atmospheric condition, the aerodynamic resistance to vapor transfer is equal to the aerodynamic resistance to heat transfer, a relationship that led to a simplification of the modified psychrometer constant and hence to the common form of the Penman-Monteith system of equations (e.g., Monteith and Unsworth, 2013). Although the focus in evaporation studies is mainly on the transfer of vapor and sensible heat from a canopy complex to the air above, the convective transfer of momentum is also integral (and hence inextricably coupled) to the evaporation process. Thus, in Chapter 3, the equation for the aerodynamic resistance to momentum transfer is derived and the relationship

between the resistance parameters to the convective transfer of momentum and that of vapor/heat is explored. The chapter closes with a description of the equation widely used to estimate the aerodynamic resistance to vapor/heat transfer and with a reference to a method used for estimating the bulk surface resistance in agricultural water management applications.

The equations for latent heat flux, sensible heat flux, and the final air temperature derived in Chapter 2 consist of a coupled set, because the value of the slope parameter relating to the saturation vapor pressure curve,  $\Delta$ , is not known *a priori*. The development and evaluation of numerical solutions to the Penman-Monteith system of equations is presented in Chapter 4. Four alternative algorithms with varying degrees of complexity (referred to as model 1, 2, 3, and 4) are described. Results of model evaluation showed that each of the alternative models produced outputs that are essentially identical and also in close agreement with a reference solution. Furthermore, intercomparison of the alternative models based on the criteria of numerical efficiency and robustness suggests that each model represents a comparable alternative, to any of the other models, for estimating evaporation. However, owing to its simplicity, model 1 is selected for further analysis.

A comparison of the outputs of model 1 with those of the conventional model (i.e., the approach widely used to evaluate the Penman-Monteith and related equations) shows that differences, in the solution techniques implemented, in the two models has maximum effect on sensible heat flux estimates (where the mean absolute residual is 18.1%), a negligible effect on estimates of the final air temperature (with an average residual of 0.7%), and a limited effect on latent heat flux estimates, in which the mean residual is 8.2%.

Both model 1 and the conventional model involve a level of approximation in the determination of  $\Delta$  and hence a direct comparison of the two models cannot provide an answer to the question: which model is more accurate? In other words, the study presented in this report does not address the question of accuracy directly. However, the relatively small mean absolute residual (of 8.2%) for latent heat flux,  $\ell_f$ , suggests that differences between the  $\ell_f$  estimates obtained with model 1 and the conventional model should typically be within the margin of error of the conventional model (the more widely used of the two models compared here). This observation suggests that, from the perspective of agricultural water management applications, both the conventional model and model 1 can, on the average, be considered equally valid descriptions of evaporation from a cropped field.

A cautionary note is, nonetheless, in order here. Although the data used in the analysis presented in this report cover a range of evaporation scenarios, they are limited and hence a conclusive deduction on this may need to await a more comprehensive follow up study focused on a comparative evaluation of model 1 and the conventional model.

## **Chapter 2. Derivation of the Penman-Monteith system of equations with the thermodynamic approach: A review and theoretical development**

### **2.1. Introduction**

Evaporation from a cropped field is a complex physical process controlled by the interplay of weather, crop, and soil factors (Penman, 1948). A comprehensive physically based modeling of evaporation from a soil-canopy system requires a numerical solution of the equations describing the coupled processes of soil-water dynamics and the transfer and transport of vapor, heat, and momentum through the soil-crop-atmosphere continuum, taking into account wind induced

advection and forced and free convection. Such a model is complex and demanding in terms of the type, resolution, and volume of input data it requires. The resources needed for acquiring and maintaining one for use in routine estimation of evaporation could also be prohibitive.

Typically, for agricultural water management purposes, steady-state evaporation is computed with explicit equations as a function of, time averaged, measurable weather data. Equations of evaporation are developed based on varying degrees of approximations regarding the dominant factors and mechanisms that derive the vapor and heat transfer processes from the soil-canopy complex to the atmosphere. For instance, the Bowen ratio method, a method based on surface energy balance principles, is used to estimate evaporation from measurements of net solar radiation, soil heat flux, and gradients of air temperature and vapor pressure (Brutsaert, 1982; Monteith and Unsworth, 2013; Jensen and Allen, 2016). The aerodynamic method (e.g., Thornthwaite and Holzman, 1942) defined in terms of vapor pressure and wind speed is another approach for evaporation estimation from measured weather data. Additional empirical approximations that rely on limited sets of weather data for use in areas where a complete set is unavailable exist (Doorenbos and Pruitt, 1977).

An equation that combines the energy balance and aerodynamic components was derived by Penman (1948). Monteith (1965) extended the Penman equation into the form widely known as the Penman-Monteith equation, which has the same general form as its precursor, but involves partitioning of the leaf-boundary-layer resistance to vapor transfer into: *(i)* stomatal resistance for an isolated single leaf or canopy resistance for a uniform stand of vegetation and *(ii)* resistance to the transfer of vapor across the turbulent boundary layer. The Penman-Monteith equation is generally considered as the most comprehensive steady-state evaporation equation and as such it

was recommended as the standard method by FAO (Allen et al., 1998) and ASCE (Jensen and Allen, 2016).

A survey of the literature suggests that there are two approaches to the derivation of the Penman-Monteith equation. The most widely used approach (e.g., Jensen and Allen, 2016), broadly patterned after that of Penman (1948), generally considers evaporation as a vapor, heat, and momentum transfer process between a source/sink surface and a point (at measurement height) in the ambient air current. The rate (of vapor or heat) transfer is directly proportional to the respective potential differences and inversely related to the resistances across the points. During evaporation, the temperature of the exchange surface is considered constant. While the interface between the surface and the ambient air is presumed saturated, the air is generally considered unsaturated, although this may not necessarily be a requirement.

An alternative approach proposed by Monteith (1965, 1981), on the other hand, conceptualizes evaporation as a physical process that produces changes in the thermodynamic state of the ambient air. A formulation that allows evaporation to be described in terms of (or from the vantage point of) the changes it introduces into the energy states of a thermodynamic system. Accordingly, a stationary air parcel that exchanges vapor and heat only with a source/sink surface is considered here to constitute a thermodynamic system. The approach proposes a framework in which evaporation is defined in terms of a pair of formal thermodynamic subprocesses (consisting of adiabatic cooling and diabatic heating) that leads to an increase/a decrease in the (energy) state of the air parcel in ways that are readily quantifiable. Overall, the conventional approach to the derivation of the Penman-Monteith equation (e.g., Jensen and Allen, 2016) has the advantage of being mathematically straight forward and compact. The thermodynamic approach (Monteith, 1981), on the other hand, has the benefit of

revealing of key assumptions and concepts that are generally implicit in the conventional approach.

This chapter derives the Penman-Monteith equation following the thermodynamic conceptualization of the evaporation process (Monteith, 1981). While essentially reviewing Monteith's approach, the development here lists a specific set of assumptions that the derivation is based on, attempts to fill gaps (mainly in terms of providing extended discussion in places where the original discussion was succinct), and emphasizes interpretations of the mathematical/physical attributes of the terms and parameters of the Penman-Monteith equation. The resultant equations for latent heat flux, sensible heat flux, and the final air temperature, referred here as the Penman-Monteith system of equations, consist of a coupled set. Thus, the development and evaluation of numerical solutions, to this system of equations, is presented in Chapter 4.

## **2.2. Evaporation as a thermodynamic process and assumptions**

Unlike the conventional approach, where evaporation is treated as vapor and heat transfer process between two points in space (i.e., a point in the exchange surface and another one in the air current), the thermodynamic conceptualization of evaporation introduces a perspective whereby the process can be studied from the vantage point of the changes it produces in the thermodynamic properties (specifically, the latent heat and sensible heat contents) of the ambient air. Following Monteith (1965, 1981), natural evaporation is, thus, described here in terms of a pair of formal thermodynamic subprocesses (namely, adiabatic cooling and diabatic heating) that

modify the energy state of a suitably defined thermodynamic system (to be specified subsequently) in ways that are readily quantifiable.

Accordingly, the Penman-Monteith equation is deduced in two steps. First, a form of the equation that models evaporation into a stationary ambient air from a wet surface is obtained based on analysis of the changes in the thermodynamic states of the air parcel using equations of state. In a subsequent step, resistance parameters are introduced into the basic equations, accounting for the dynamic effects of wind-surface interactions and those of (bulk) canopy system response to atmospheric conditions, on evaporation, leading to the Penman-Monteith equation.

The following set of assumptions are introduced here as the basis to the derivation of the Penman-Monteith equation with the thermodynamic approach. *(i)* The thermodynamic system consists of an air parcel, of given mass and specified vapor pressure and temperature, that neither mixes nor exchanges heat and vapor with the surrounding air, but exchanges vapor and heat with a source/sink surface that it is in contact with. Analyses based on air parcels of indeterminate form and shape are widely used in thermodynamic studies of the atmosphere in meteorology (e.g., Monteith, 1981; Arya, 1991). The presumption here is that observations deduced on the evaporation process involving a suitably defined system, based on analysis of the changes in the thermodynamic states of the system, can be generalized for the ambient air spanning the entire evaporative surface; *(ii)* The analysis considers an idealized (virtual) surface as the effective source/sink for vapor and heat and such a surface is termed here as the exchange surface, or simply as, the surface; *(iii)* The exchange surface has no mass and heat capacity (e.g., Arya, 1991) and hence it cannot store thermal energy, instead energy incident on the surface in the form of solar radiation is reflected and radiated back, used to heat the sub-medium (e.g., a water

body or soil and/or crops), and used to heat the air parcel (the latter is a fraction referred here as the external heat flux into the air parcel); and (iv) The surface temperature and vapor pressure are constant during evaporation and each of the surface energy balance components represent a steady flux during an evaporation process. Furthermore, it is presumed that there exist no temperature, vapor pressure, and energy flux gradient across the surface.

## 2.3. Evaporation into a quiescent air

### 2.3.1. Description of concepts

To develop the equations for evaporation into a stationary ambient air, consider a scenario in which water evaporates, from a wet source/sink surface, into a thermodynamic system defined earlier. The thermodynamic state of such a system can be specified in terms of its latent and sensible heat contents, which in turn can be represented in terms of surrogate variables: vapor pressure,  $e$ , and temperature,  $T$ , respectively (Monteith, 1965, 1981). It, thus, follows that a vapor pressure versus temperature chart, akin to a simplified conceptual psychrometric chart, (sketched in Figure 1) can be used to describe the evaporation process into a stationary air parcel. It ought to be emphasized here that the use of elements of the psychrometric chart and related terms in the, following, description of evaporation is only conceptual.

Figure 1 depicts some useful thermodynamic states of the air and pertinent processes superimposed on the simplified conceptual psychrometric chart. Two key features of the chart are the wet-bulb temperature line,  $w(T)$  (corresponding to the initial thermodynamic state of the air, which is labeled as  $\alpha$ ,  $(T_0, e_0)$ ), and the saturation vapor pressure curve,  $e_s(T)$ . As can be noted from Figure 1, the wet-bulb temperature line contains the states  $\alpha$  and  $\beta$ ,  $(T_w, e_s(T_w))$ , and the negative of its slope,  $\gamma$  (KPa/K), is the psychrometer constant. The saturation vapor pressure

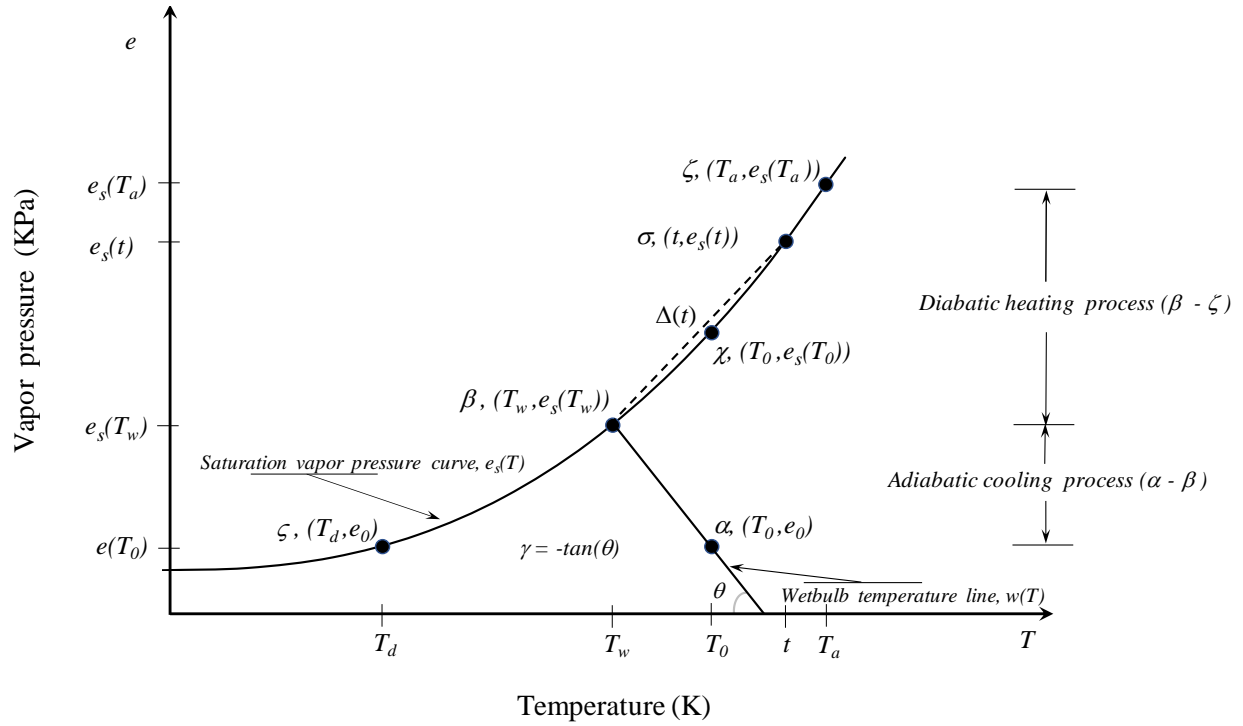


Fig 1. A simplified conceptual psychrometric chart depicting adiabatic cooling of the air parcel (from state  $\alpha$  to  $\beta$ ) and diabatic heating of the air in a state of saturation (from  $\beta$  to  $\zeta$ ). Note:  $T$  (K) is temperature,  $T_d$  (K) is the dewpoint temperature,  $T_w$  (K) is the wet-bulb temperature,  $T_0$  (K) is the measured air temperature,  $t$  (K) defines variable air temperature in the range  $T_w \leq t \leq T_a$ ,  $e_s$  (kPa) is saturated vapor pressure at a specified temperature,  $e_0$  or  $e(T_0)$  (kPa) is measured vapor pressure, and  $\gamma$  is the psychrometer constant (kPa/K), and  $\Delta$  is the slope of the line connecting states  $\beta$  and  $\zeta$

curve, on the other hand, contains the points  $\varsigma$ ,  $\beta$ ,  $\chi$ ,  $\sigma$ , and  $\zeta$ . Points  $\varsigma$ ,  $\beta$ ,  $\chi$ , and  $\zeta$  define states of saturation, of the air parcel, at the dewpoint temperature,  $T_d$ , wet-bulb temperature,  $T_w$ , the measured air temperature,  $T_0$ , and the final air temperature,  $T_a$ , respectively. Furthermore, the point  $\sigma$ ,  $(t, e_s(t))$ , is a state of saturation at some temperature  $t$ , where  $T_w \leq t \leq T_a$ , and  $\Delta(t)$  is the slope of the line connecting state  $\beta$  with that of  $\sigma$ , which is a key parameter in simplifying the resultant equation. In Figure 1, the final air temperature,  $T_a$ , is greater than the measured dry-bulb temperature,  $T_0$ , however, it needs to be pointed out here that this is not a requirement.

Noting that points  $\alpha$ ,  $(T_0, e_0)$ , and  $\zeta$ ,  $(T_a, e_s(T_a))$ , are the initial and final thermodynamic states, respectively, of the air parcel, it can be observed that the change in the thermodynamic state of the air from  $\alpha$  to that of  $\zeta$  involves change in the total heat content (i.e., the sum of the sensible and latent heat) of the air parcel. Energy differential between two states of a thermodynamic system is independent of the path taken and depends only on the initial and final states of the system defined by the thermodynamic properties (e.g., Rajput, 2007). Based on this principle, Monteith (1965) proposed a conceptual framework that describes the physics underlying natural evaporation, from a wet surface into a moist air parcel of specified vapor pressure and temperature, in terms of a pair of formal thermodynamic subprocesses (Figure 1), consisting of adiabatic cooling of the air driven by sensible heat extant in the air at the start of evaporation and diabatic heating in a state of saturation caused by external heat flux from the surface. Note that implicit in this description is the assumption that conversion of heat into work done by the air parcel is considered negligible, possibly on account of the consideration that evaporation takes place under constant pressure and the variation in air temperature (during evaporation) is sufficiently small for the density of the air parcel to be adequately represented by an average value. Thus, it is important to note here that description of air density here refers to a constant average value over the evaporation process.

Adiabatic cooling of a moist, yet unsaturated air parcel, is depicted in Figure 1 by the path connecting states  $\alpha$  and  $\beta$  along the wet-bulb temperature line,  $w(T)$ . It can be observed from Figure 1 that the sensible heat extant in the air parcel at the start of evaporation (state  $\alpha$ ) is steadily reduced, resulting in a corresponding decrease in the air temperature from that of the measured temperature,  $T_0$ , towards the wet-bulb temperature,  $T_w$ . However, heat does not cross the boundary of the air parcel (adiabatic process), instead it is used to evaporate water from the

wet boundary of the parcel, resulting in an increase in the latent heat content of the air parcel and hence its vapor pressure from  $e(T_0)$  towards  $e_s(T_w)$ . It thus follows, in the adiabatic process, the reduction in the sensible heat content of the air parcel is exactly balanced by the gain in latent heat. The processes of adiabatic cooling and humidifying of the air parcel continue eventually leading to saturation at the wet-bulb temperature,  $e_s(T_w)$ , which is represented by the thermodynamic state,  $\beta$ .

By contrast, the diabatic heating process is represented by the path connecting states  $\beta$  and  $\zeta$  along the saturation vapor pressure curve,  $e_s(T)$ , and involves both vapor and heat transfer between the exchange surface and the air parcel. For the scenario considered in Figure 1, where  $T_a > T_w$ , the external heat flux into the air parcel provides the energy that leads to heating of the air in a state of saturation. In other words, under the scenario in which  $T_a$  exceeds  $T_w$ , both the sensible heat and latent heat contents of the air parcel and its temperature and vapor pressure would increase.

If, on the other hand, the final air temperature is less than the wet-bulb temperature, i.e.,  $T_w > T_a$ , it can then be observed from Figure 1 that diabatic cooling would occur. In other words, there would occur an outflow of both sensible and latent heat from the air parcel, leading to a decrease in the sensible and latent heat contents of the air parcel. However, for simplicity, the derivation presented here will be based on the assumption that  $T_a > T_w$ . It can be shown that the form of the equation obtained as such is directly applicable to the scenario where  $T_w > T_a$ , the only requirement is that the external heat flux needs to have a negative algebraic sign, indicating that the air parcel is losing heat to the exchange surface. Notably, a close look at the simplified conceptual psychrometric chart reveals that evaporation can occur even when the final air temperature,  $T_a$ , is less than the measured air temperature,  $T_0$ , provided  $T_a$  is greater than the

dewpoint temperature. It will be shown later that the final air temperature is equal to the surface temperature.

Note that evaporation is considered here as a steady-state process. It is, therefore, important to observe that the adiabatic cooling and diabatic heating processes should not be perceived as consecutive thermodynamic phases in time. They are only used in the conceptual definition of evaporation in terms of the constituent thermodynamic subprocesses, the identification of corresponding sources of heat, and specification of the changes in the states of the system in ways that are readily quantifiable. The preceding formulation of natural evaporation as a thermodynamic process (Monteith, 1981) will now be used in subsequent derivation of the Penman-Monteith equation.

### **2.3.2. Equations**

The preceding discussion summarizes the thermodynamic formulation of the evaporation process using a relatively simple, and more familiar, conceptual chart that defines the state of the system in terms of vapor pressure,  $e$ , and temperature,  $T$ . However, Monteith (1981) used a conceptual two-dimensional chart (that specifies the thermodynamic states of an air parcel in terms of its latent heat and sensible heat contents per unit mass) to derive a form of the Penman-Monteith equation that models evaporation into a stationary ambient air (of specified  $e_0$  and  $T$ ) from a wet exchange surface. Here, on the other hand, the analysis is based on the latent heat,  $q(T)$ , and sensible heat,  $\ell(T)$ , contents of a unit volume of the air parcel, Figure 2. This is predicated on the consideration that evaporation takes place under constant pressure and the range of temperature changes during evaporation (i.e., the interval between  $T_w$  and  $T_a$ ) are sufficiently small for

volume variations to be considered not significant and hence for the air density to be represented adequately in terms of an average value.

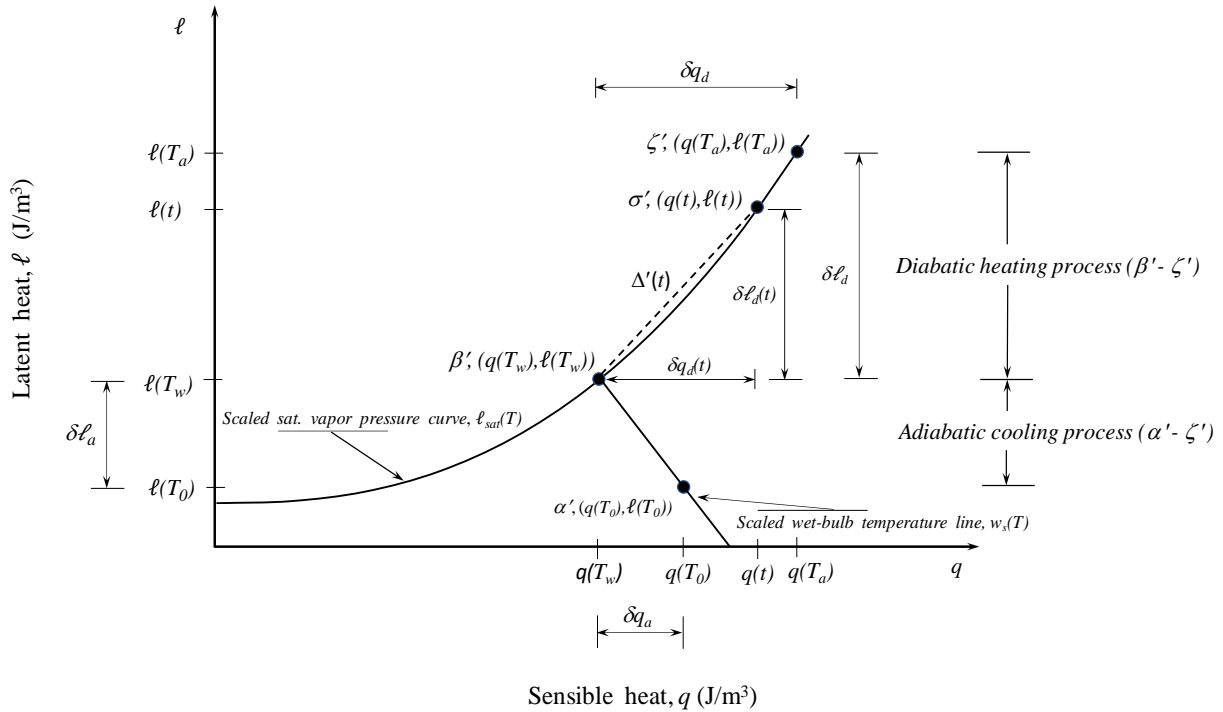


Fig 2. Simplified chart depicting the thermodynamic states of an air parcel in an evaporation process (sensible heat and latent heat content space, adapted from Monteith, 1981).  $\ell$  and  $q$  are latent heat and sensible heat content of a unit volume of air ( $\text{J/m}^3$ ), respectively; the subscripts  $a$  and  $d$  represent adiabatic and diabatic processes, respectively;  $\alpha'$ ,  $\beta'$ ,  $\sigma'$ , and  $\zeta'$  are thermodynamic states of the air, in the  $\ell$ - $q$  space, corresponding to those of  $\alpha$ ,  $\beta$ ,  $\sigma$ , and  $\zeta$  in the  $e$ - $T$  space. Note:  $\Delta'$  is equal to  $\Delta$  in the  $e$ - $T$  space scaled by the reciprocal of the psychrometer constant

A close look at Figure 2, in light of the unique dependence of  $\ell$  and  $q$  on temperature,  $T$ , along the  $w_s$  line and the  $\ell_{sat}$  curve, reveals that Figure 2 represents a scaled version of the conceptual psychrometric chart, depicted in Figure 1, where the scaling constants are  $\rho c_p$  for the abscissa and  $\lambda \rho \epsilon / p$  for the ordinate (note that the parameters  $c_p$ ,  $\lambda$ ,  $\rho$ ,  $\epsilon$ , and  $p$  are defined shortly in relation to Eq. 1). It can, thus, be observed that there is a one-to-one mapping between the thermodynamic states in Figure 1 and those of Figure 2. Accordingly, it can be observed that

states  $\alpha'$ ,  $\beta'$ ,  $\sigma'$ , and  $\zeta'$  in Figure 2 correspond to states  $\alpha$ ,  $\beta$ ,  $\sigma$ , and  $\zeta$  in Figure 1, respectively.

The adiabatic cooling process is represented by the path connecting states  $\alpha'$  and  $\beta'$  along the  $w_s$  line and diabatic heating of the air parcel, while maintaining saturation, is represented by the path connecting  $\beta'$  and  $\zeta'$  along the  $\ell_{sat}$  curve. Furthermore, the  $\Delta'(t)$  parameter represents the slope of the line connecting states  $\beta'$  and  $\sigma'$  at some temperature  $t$ , where  $T_w \leq t \leq T_a$ .

The thermodynamic equation of state for latent heat,  $\ell(T)$ , can now be defined along the scaled wet-bulb temperature line,  $w_s$ , and the scaled saturation vapor pressure curve,  $\ell_{sat}$ , as

$$\ell(T) = \lambda \rho \xi(T), \quad \text{where} \quad \xi = \frac{\epsilon}{(p - e) + \epsilon e} e(T) \approx \left(\frac{\epsilon}{p}\right) e(T) \quad (1)$$

Similarly, the equation of state for sensible heat,  $q(T)$ , can be given as

$$q(T) = \rho c_p T \quad (2)$$

where  $\ell(T)$ ,  $\text{J/m}^3$ , and  $q(T)$ ,  $\text{J/m}^3$ , are latent heat and sensible heat contents per unit volume of the air parcel, respectively;  $\rho$  ( $\text{Kg/m}^3$ ) is the density of air;  $\lambda$  ( $\text{J/Kg}$ ) is the latent heat of vaporization of water;  $\xi$  ( $\text{Kg-vapor/Kg-moist-air}$ ) is the specific humidity of the air;  $\epsilon$  (-) is the ratio of the molar mass of vapor to that of dry air and is set to 0.622;  $p$  ( $\text{KPa}$ ) is air pressure;  $e$  ( $\text{KPa}$ ) is vapor pressure;  $c_p$  ( $\text{J/Kg-K}$ ) is the specific heat of air at constant pressure; and  $T$  ( $\text{K}$ ) is temperature.

The change in the latent heat content of a unit volume of the air parcel,  $\delta\ell$  ( $\text{J/m}^3$ ), during evaporation, can be expressed as the sum of the adiabatic,  $\delta\ell_a$ , and diabatic,  $\delta\ell_d$ , components

$$\delta\ell = \delta\ell_a + \delta\ell_d \quad (3)$$

Similarly, the corresponding change in the sensible heat content of a unit volume of the air parcel,  $\delta q$  ( $\text{J}/\text{m}^3$ ), can be given as the sum of the adiabatic,  $\delta q_a$ , and diabatic,  $\delta q_d$ , fractions

$$\delta q = \delta q_a + \delta q_d \quad (4)$$

Expressions for the changes in the latent heat,  $\delta \ell$ , and sensible heat,  $\delta q$ , contents of a unit volume of the air parcel as a function of readily measurable weather parameters will now be derived.

### ***2.3.2.a. Evaporation into a moist but unsaturated air, adiabatic cooling process***

Consider an air parcel that is cooled from the measured air temperature,  $T_0$ , to its wet-bulb temperature,  $T_w$ , adiabatically, while its vapor pressure is increased from  $e_0$  (or  $e(T_0)$ ) to  $e_s(T_w)$ , which is represented by the path between  $\alpha'$  and  $\beta'$  in Figure 2. As noted earlier, in the adiabatic process, the changes in the latent heat and sensible heat contents of a unit volume of the air parcel ( $\delta \ell_a$  and  $\delta q_a$ , respectively) are equal in magnitude, but are of opposite algebraic sign. Thus, the heat balance of the air parcel, for the adiabatic process, can be given as

$$\delta \ell_a + \delta q_a = 0 \quad (5)$$

The decrement in the sensible heat content of a unit volume of the air parcel,  $\delta q_a$ , defined along the path  $\alpha'$  to  $\beta'$  can be expressed as

$$\delta q_a = \rho c_p (T_w - T_0) \quad (6)$$

The corresponding increment in the latent heat content of a unit volume of the air parcel,  $\delta\ell_a$ , can be given as

$$\delta\ell_a = \frac{\lambda\rho\epsilon}{p}(e_s(T_w) - e_0) \quad (7)$$

Equations 6 and 7 represent potential differences between the initial and final thermodynamic states defining the adiabatic cooling process. Noting that the dry-bulb temperature can be measured more readily and accurately than the wet-bulb temperature, an equation that relates the change in the latent heat content of the air parcel in the adiabatic process,  $\delta\ell_a$ , with the vapor pressure deficit at the measured temperature,  $T_0$ , will now be presented.

Noting that  $\delta\ell_a = -\delta q_a$  (from Eq. 5) and equating the negative of the righthand side of Eq. 6 with that of Eq. 7 and simplifying the resultant expression yields

$$e_s(T_w) - e_0 = \gamma(T_0 - T_w), \quad \text{where } \gamma = \frac{pc_p}{\lambda\epsilon} \quad (8)$$

Another key parameter (i.e., in addition to  $\gamma$ ), which is labeled in Figure 2 as  $\Delta'(t)$  and represents the slope of a linear equation that relates point  $\beta'(q(T_w), \ell(T_w))$  on the  $\ell_{sat}(T)$  curve with any other point,  $\sigma'(q(t), \ell(t))$ , on the same curve will now be introduced

$$\ell_{sat}(T_w) = \ell_{sat}(t) - \Delta'(t)(q(t) - q(T_w)) \quad (9)$$

where  $t$  is a temperature that varies in the range  $T_w \leq t \leq T_a$ . Substituting  $\lambda\rho\epsilon e_s(T)/p$  for  $\ell_{sat}$  and  $\rho c_p T$  for  $q$  into Eq. 9 and simplifying yields

$$e_s(T_w) = e_s(t) - \Delta'(t)\gamma(t - T_w) \quad (10)$$

Based on the definition of the slope of a line, it can be shown that  $\Delta'(t)$  is equal to  $\Delta(t)$  (Figure 1) scaled by the reciprocal of the psychrometer constant

$$\Delta'(t) = \frac{\Delta(t)}{\gamma} \quad (11)$$

Combining Eqs. 10 and 11 and simplifying yields

$$e_s(T_w) = e_s(t) - \Delta(t)(t - T_w) \quad (12)$$

Furthermore, substituting the right-hand side of Eq. 12 into Eq. 8 and rearranging terms yields

$$e_s(t) - e_0 = \Delta(t)(t - T_w) + \gamma(T_0 - T_w) \quad (13)$$

Setting  $t = T_0$  and rearranging results in

$$T_0 - T_w = \frac{e_s(T_0) - e_0}{\Delta(T_0) + \gamma} \quad (14)$$

Note that Eq. 14 is an exact expression, provided  $\Delta(T_0)$  is evaluated at an appropriate temperature,  $\tau$ , such that

$$\Delta(T_0) = \left. \frac{\partial e_s(T)}{\partial T} \right|_{T=\tau}, \quad \text{where } T_w \leq \tau \leq T_0 \quad (15)$$

Combining Eqs. 14 and 6 and then substituting  $\Delta_a$  for  $\Delta(T_0)$  in the resultant expression (while noting that in the adiabatic cooling process,  $\delta\ell_a = -\delta q_a$ ), yields the expression for  $\delta\ell_a$  in terms of the measured air temperature

$$\delta\ell_a = \rho c_p \frac{e_s(T_0) - e_0}{\Delta_a + \gamma} \quad (16)$$

The righthand side of Eq. 16 is the adiabatic term of a form of the Penman-Monteith equation that models evaporation from a wet surface into a quiescent ambient air. Remarkably, it can be shown, based on the concept of wet-bulb temperature (e.g., Monteith and Unsworth, 2013), that Eq. 16 is of the same form as the expression for latent heat associated with an isolated system cooled adiabatically to its thermodynamic wet-bulb temperature.

### ***2.3.2.b. Evaporation into saturated air, diabatic heating in a state of saturation***

In contrast to the adiabatic cooling process, in the diabatic heating process heat transfer between the exchange surface and the air parcel is permissible. As noted earlier, in the scenario considered here (where  $T_a > T_w$ ), diabatic heating (driven by a steady external heat flux into the air) leads to an increase in both the sensible and latent heat contents of the air parcel and hence to a change in the thermodynamic state of the air parcel from that of  $\beta'(T_w, e_s(T_w))$  to  $\zeta'(T_a, e_s(T_a))$  along the scaled saturation vapor pressure curve, Figure 2. It, thus, follows that the answer to the question of finding an expression for the change in the latent heat content of the air (along the path  $\beta'$  to  $\zeta'$ ) boils down to the determination of the proportionality factor with which the external heat flux, which is given, is partitioned into latent and sensible heat contents.

It follows from the preceding discussion that the heat balance of the air parcel in the diabatic process can be given as

$$Q = \delta\ell_d + \delta q_d \tag{17}$$

where  $Q$  is the external heat input into a unit volume of the air parcel, which leads to a change in the total heat content of the air parcel ( $\text{J}/\text{m}^3$ ). As can be noted from Figure 2,  $\delta\ell_d$  ( $\text{J}/\text{m}^3$ ) and  $\delta q_d$

(J/m<sup>3</sup>) are, respectively, increments in the latent heat and sensible heat contents of a unit volume of the air parcel as it is heated in a state of saturation.

Considering a linear equation (of the form given in Eq. 9) that relates the point  $\beta'(T_w, e_s(T_w))$  on the scaled saturation vapor pressure curve with that of  $\zeta'(T_a, e_s(T_a))$ , it can be shown that  $\Delta'(T_a) = \Delta(T_a)/\gamma$ . Furthermore, a close look at Figure 2 shows that  $\delta\ell_d/\delta q_d = \Delta(T_a)/\gamma$ . Now, combining the expression  $\delta\ell_d/\delta q_d = \Delta(T_a)/\gamma$  with Eq. 17 and substituting the notation  $\Delta_d$  for  $\Delta(T_a)$  results in

$$\frac{\Delta_d}{\gamma} = \frac{\delta\ell_d}{\delta q_d} = \frac{\delta\ell_d}{Q - \delta\ell_d} \quad (18)$$

Simplifying, yields

$$\delta\ell_d = \frac{\Delta_d Q}{\Delta_d + \gamma} \quad (19)$$

### ***2.3.2.c. Combined equations: A form of the Penman-Monteith equation that models evaporation into a stationary ambient air from a wet surface and related equations***

The linear equation given in Eq. 12 (in relation to which the slope parameters,  $\Delta_a$  and  $\Delta_d$ , are defined) is an exact expression, provided  $\Delta_a$  and  $\Delta_d$  are computed subject to the requirement stated in Eq. 15. However, in the interest of keeping the resultant equation for  $\delta\ell$  simpler, it is assumed here that an effective average  $\Delta$ , somewhere in the interval  $[\Delta_a, \Delta_d]$ , can be used in place of both  $\Delta_a$  and  $\Delta_d$ . Note that this is predicated on the assumption that the temperature interval,  $T_a - T_0$ , during a natural evaporation process is sufficiently small, such that  $\Delta_a$  is close enough to  $\Delta_d$ , and hence a constant,  $\Delta$ , can be used in place of  $\Delta_a$  and  $\Delta_d$  without compromising accuracy.

Substituting  $\Delta$  for  $\Delta_a$  and  $\Delta_d$  in Eqs. 16 and 19, respectively, and combining the resultant expressions with the equation for  $\delta\ell$  (Eq. 3) yields the change in the latent heat content of a unit volume of a stationary air parcel during an evaporation process from a wet surface

$$\delta\ell = \frac{\Delta Q}{\Delta + \gamma} + \rho c_p \frac{e_s(T_0) - e_0}{\Delta + \gamma} \quad (20)$$

Note that alternative methods for computing  $\Delta$  are presented in Chapter 4.

Following the same approach as that used to deduce the equation for  $\delta\ell_d$  (Eqs. 17 to 19), it can be shown that the expression for  $\delta q_d$  ( $\text{J/m}^3$ ) can be given as

$$\delta q_d = \frac{\gamma Q}{\Delta + \gamma} \quad (21)$$

Substituting Eq. 21 and the negative of Eq. 16 into Eq. 4 yields the overall change in the sensible heat content of a unit volume of the air parcel,  $\delta q$ ,

$$\delta q = \frac{\gamma Q}{\Delta + \gamma} - \rho c_p \frac{e_s(T_0) - e_0}{\Delta + \gamma} \quad (22)$$

An equation for the final temperature of the air parcel,  $T_a$ , can be deduced by combining Eq. 22 with a form of the sensible heat equation (Eq. 6), in which the temperatures corresponding to the initial and final states of the air parcel are set to  $T_0$  and  $T_a$ , respectively.

$$T_a = T_0 + \frac{\gamma Q}{\rho c_p (\Delta + \gamma)} - \frac{e_s(T_0) - e_0}{\Delta + \gamma} \quad (23)$$

In the development of Eqs. 20, 22, and 23, evaporation is treated as a process of vapor and heat transfer from a wet exchange surface into a stationary ambient air. However, natural evaporation from a cropped field, where water availability is not a limiting factor, occurs under a more complex set of conditions. Typically, there is advective transport due to wind; interaction between wind and the crop-canopy system which leads to the convective transport of momentum, heat, and vapor (vertically) by turbulent eddies; and (bulk) crop-canopy system effects, which includes crop-physiological response to atmospheric conditions but not limited to it. The Penman-Monteith equation will now be developed accounting for these effects, although in an approximate sense.

## **2.4. The Penman-Monteith equation**

### **2.4.1. Evaporation described in terms of sensible heat and latent heat flux space and equations**

In subsequent development, we will continue to make use of Monteith's formulation that frames evaporation as a thermodynamic process that can be described by tracking the changes in the state of a stationary air parcel, of given mass and vapor pressure and temperature, in contact with an exchange surface. The assumptions made earlier regarding the modes of interaction of the air parcel with the exchange surface and the surrounding air remains in place. In addition, the consideration, indicated earlier, that natural evaporation occurs under constant air pressure and that the range of variation of temperature is limited (hence the variation in the density of the air is sufficiently small to be represented adequately by an average value) holds here as well.

Furthermore, the following simplifying assumptions are introduced here as the basis to the development of the Penman-Monteith equation accounting for the dynamic effects of wind

and canopy system effects on natural evaporation: (i) A cropped field with a uniform stand, optimal vegetative growth, and no limitations in the availability of water is considered, thus, evaporation occurs at the potential rate; (ii) Virtual surfaces, situated within the crop canopy, serve as effective sink for momentum, on one hand, and source/sink for vapor and heat, on the other; (iii) The turbulent transport of vapor, heat, and momentum between the exchange surfaces and the ambient air produced mainly by wind-surface interaction effects and bulk canopy system response (to atmospheric conditions) are considered the principal coupled mechanisms that control evaporation; (iv) The convective transport of heat and vapor between the source/sink surface and the air and the effects of the (bulk) canopy system response to atmospheric conditions can be modelled sufficiently accurately by combining the equations for potential difference (defined in terms of the thermodynamic equations of state, Eqs. 1 and 2), with an appropriate set of resistance parameters; and (v) The cropped field covers a sufficiently expansive area (with negligible edge effect) and hence the transfer of physical quantities of interest is one-dimensional in the vertical direction.

Evidently, the introduction of the transfer parameters into the basic equations implies that the interest here is not cumulative heat gains/losses by the air parcel during an evaporation process, as was the case in the preceding development. Instead, it is in heat fluxes into/from the air parcel in the diabatic process and of course in the rate of conversion of thermal energy (from sensible heat to latent heat) within the air parcel in the adiabatic process. Accordingly, following Monteith (1981), Figure 2 will now be mapped onto a two-dimensional space in which the abscissa is sensible heat flux,  $q_f(T)$  ( $\text{W}/\text{m}^2$ ), and the ordinate will be latent heat flux,  $\ell_f(T)$  ( $\text{W}/\text{m}^2$ ), as shown in Figure 3. Note that Monteith (1981) did not specifically present Figure 3 in any form, but described its features and applied them to deduce the Penman-Monteith equation.

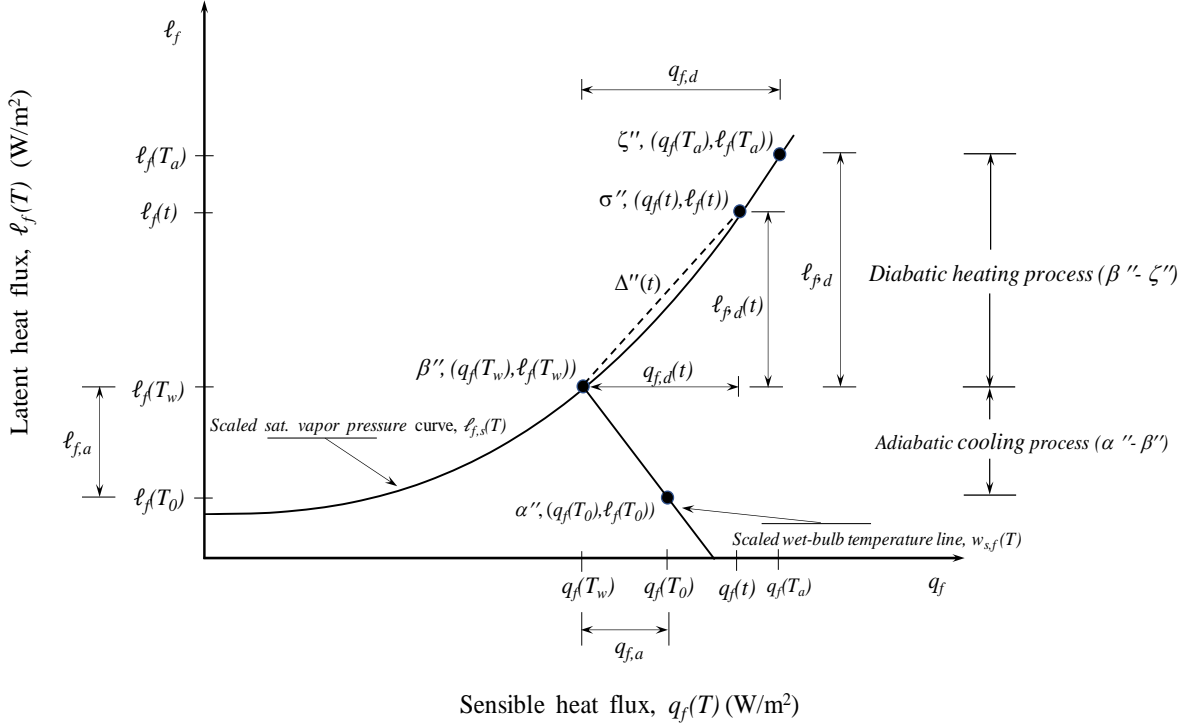


Figure 3. Simplified chart depicting the thermodynamic states of an air parcel in an evaporation process (sensible and latent heat flux space).  $\ell_f$  and  $q_f$  are the latent heat and sensible heat fluxes ( $\text{W/m}^2$ ), respectively; the subscripts  $a$  and  $d$  represent adiabatic and diabatic processes, respectively;  $\alpha''$ ,  $\beta''$ ,  $\sigma''$ , and  $\zeta''$  are thermodynamic states of the air, in the  $\ell_f$ - $q_f$  space, corresponding to those of  $\alpha$ ,  $\beta$ ,  $\sigma$ , and  $\zeta$  in the  $e$ - $T$  space; and it will be shown later that  $\Delta''$  is equal to  $\Delta$  in the  $e$ - $T$  space scaled by the reciprocal of the modified psychrometer constant

Along the scaled wet-bulb temperature line,  $w_{s,f}$ , and that of the scaled saturation vapor pressure curve,  $\ell_{f,s}$ , of Figure 3, the latent heat and sensible heat fluxes can be expressed as

$$q_f(T) = \frac{q(T)}{r_h} \quad \text{and} \quad \ell_f(T) = \frac{\ell(T)}{r_v} \quad (24)$$

In Eq. 24,  $q(T)$ ,  $\text{J/m}^3$ , and  $\ell(T)$ ,  $\text{J/m}^3$ , are latent and sensible heat contents of a unit volume of the air parcel, respectively, defined in terms of Eqs. 1 and 2, and  $r_h$  (s/m) and  $r_v$  (s/m) are parameters

representing resistance to heat and vapor transfer, respectively. Further discussion on the resistance parameters and methods used to evaluate them will be presented in Chapter 3.

#### **2.4.2. Physical interpretation of the flux equations and the use of flux as a thermodynamic property**

In principle, fluxes are defined across potential differences. However, that appears not to be the case in Eq. 24. A question that may, thus, arise here is: what physical meaning can be assigned to the fluxes defined in Eq. 24. The sensible heat flux at some temperature,  $T$ ,  $q_f(T)$  or  $q(T)/r_v$ , can be interpreted as the amount of heat that needs to flow into the air parcel, per unit area of the surface and in a unit time of interest, in order to raise the heat content of a unit volume of the air to such a level that its temperature is increased from a reference temperature (absolute zero,  $0\text{ K}$ , considered ground state) to  $T$ , given the  $r_h$  value. Similarly, the difference between two levels of the sensible heat flux, say between  $q_f(t)$  and  $q_f(T_w)$  (which is labeled as  $q_{f,d}(t)$  in Figure 3), represents the quantity of heat that must flow into the air parcel (across a unit area of the surface and in a unit time of interest) so as to raise the heat content of a unit volume of the air by such an amount that its temperature is increased from  $T_w$  to  $t$ , given the resistance parameter. Note that same observation can be made with regard to the latent heat flux defined in Eq. 24.

Another point that may require a closer examination here is the use of fluxes as state variables, which appears unconventional. Given that fluxes are not intrinsic properties of the air parcel, a question might be raised about the implications of using fluxes as state variables.

Although Figure 3 is less intuitive than that of Figure 2, it can be shown that there is a one-to-one mapping between the set of points in Figures 3 and that of Figure 2 and as such Figure 3 can be

considered as an equally valid representation of the thermodynamic states of the air parcel as that of Figure 2.

As noted earlier, it is the unique dependence of latent heat,  $\ell(T)$ , and sensible heat,  $q(T)$ , contents of the air on temperature (along the wet-bulb temperature and the saturation vapor pressure curve) that forms the basis of the relationship between Figures 1 and 2. It will now be shown that this property remains unchanged following the transformation involving the multiplication of  $\ell(T)$  and  $q(T)$  by the reciprocals of the respective resistance parameters, Figure 3.

For practical purposes, the resistance parameters,  $r_v$  and  $r_h$ , can generally be considered independent of temperature, and hence presumed constant for a given crop and stage of development (assuming optimal conditions) and wind condition. This implies that the abscissa of Figure 3 is only a scaled version of that of Figure 2, the scaling constant being  $1/r_h$ . Hence, values on the horizontal axis of Figure 3 would simply be shifted rightwards or leftwards by a factor of  $1/r_h$  with respect to the corresponding values of the abscissa of Figure 2, depending on whether  $r_h < 1$  or  $r_h > 1$ , respectively. Similarly, the ordinate of Figure 3 is equal to the ordinate of Figure 2 scaled by a constant factor of  $1/r_v$ . It can, thus, be readily observed that there is a one-to-one mapping between the set of points constituting the two-dimensional space of Figure 2 and those of Figure 3. In other words, every point (or thermodynamic state) in Figure 2 has a counterpart (and hence can be uniquely and equally represented) in Figure 3 (for instance, states  $\alpha''$ ,  $\beta''$ ,  $\sigma''$ , and  $\zeta''$  in Figure 3 correspond to states  $\alpha'$ ,  $\beta'$ ,  $\sigma'$ , and  $\zeta'$  in Figure 2). Note that the same reasoning can be used to show that Figure 3 is simply a scaled version of Figure 1. Furthermore, it can be shown that the slope of the scaled saturation vapor pressure curve, Figure 3, is equal to the slope of the saturation vapor pressure curve, Figure 1, scaled by the reciprocal

of the modified psychrometer constant (to be defined later). This implies that the scaled saturation vapor pressure curve,  $\ell_{f,s}(T)$ , in Figure 3 has the same general behavior with respect to temperature as  $e_s(T)$ , i.e., a monotonic increasing convex function of temperature.

An important point here is that in the context of the thermodynamic conceptualization of natural evaporation, a potential difference is defined as the difference between the energy levels of the thermodynamic states of the air parcel. By contrast, in the conventional approach to the derivation of the Penman-Monteith equation, potential difference represents difference in (thermal) energy levels between two points in space, i.e., a point on the surface and another one in the air current. Thus, this raises the question whether the physical meaning assigned to the parameters  $r_v$  and  $r_h$  in the conventional formulation (as the resistance to vapor and heat transfer, respectively) and the method used to evaluate them can apply to the thermodynamic formulation. This may, perhaps, need to be looked into in some detail. However, following Monteith (1981), it is assumed here that  $r_v$  and  $r_h$  have the same physical meaning as in the conventional approach and can be evaluated with the same method as those used in the conventional approach.

### 2.4.3. Equations

The latent heat flux,  $\ell_f$  ( $W/m^2$ ), and the sensible heat flux,  $q_f$  ( $W/m^2$ ), into the air parcel during an evaporation process can be expressed as the sum of the respective adiabatic and diabatic components

$$\ell_f = \ell_{f,a} + \ell_{f,d} \quad \text{and} \quad q_f = q_{f,a} + q_{f,d} \quad (25)$$

In Eq. 25,  $\ell_{f,a}$  and  $\ell_{f,d}$  are the adiabatic and diabatic fractions, respectively, of the latent heat flux and  $q_{f,a}$  and  $q_{f,d}$  represent the components of the sensible heat flux associated with the adiabatic

and diabatic processes, respectively. The latent heat and sensible heat fluxes expressed in terms of readily measurable weather parameters (including wind speed) and crop factors will now be derived.

**2.4.3.a. Evaporation into a moist but unsaturated air: Adiabatic cooling process accounting for the convective transfer of heat and vapor and (bulk) canopy system effects**

For the adiabatic process, the flux form of the heat balance equation of the air parcel can be given as

$$\delta \ell_{f,a} + \delta q_{f,a} = 0 \quad (26)$$

Based on Eq. 24, the sensible heat flux associated with the adiabatic process,  $q_{f,a}$ , can be expressed as the quotient of the potential difference between states  $\alpha'$  and  $\beta'$ , Figure 2, and the resistance to heat transfer

$$q_{f,a} = \rho c_p \frac{T_w - T_0}{r_h} \quad (27)$$

The corresponding latent heat flux associated with the adiabatic process,  $\ell_{f,a}$ , can be expressed as

$$\ell_{f,a} = \rho c_p \frac{e_s(T_w) - e_0}{\gamma^* r_h}, \quad \text{where } \gamma^* = \gamma \frac{r_v}{r_h} \quad (28)$$

In Eq. 28,  $\gamma^*$  is the modified psychrometer constant (KPa/K) and  $\rho$ ,  $c_p$ ,  $e_s(T_w)$ ,  $e_0$ ,  $r_v$ ,  $r_h$ , and  $\gamma$  were defined earlier.

Given that evaporation is considered here as an adiabatic cooling process, heat is not crossing the boundaries of the parcel. Thus,  $q_{f,a}$  in Eq. 27 ought to be viewed as the equivalent rate at which heat needs to flow from the air parcel onto a unit area of the surface per unit time, if

the sensible heat content of a unit volume of the air parcel is to be reduced from the level at state  $\alpha'$  to that at  $\beta'$  (Figure 2) through heat efflux from the air parcel onto the surface. Note that similar interpretations can be made for the latent heat flux, Eq. 28, as well.

With the view of keeping the form of the resultant equation simple, an alternative expression that relates  $\ell_{f,a}$  with the vapor pressure deficit at the measured dry-bulb temperature,  $T_0$ , will now be derived. Noting that  $\ell_{f,a} = -q_{f,a}$  (from Eq. 26) and equating the righthand side of Eq. 28 with the negative of the righthand side of Eq. 27 and simplifying yields

$$e_s(T_w) - e_0 = \gamma^*(T_0 - T_w) \quad (29)$$

A linear equation (of the form given in Eq. 9) that relates the latent heat and sensible heat fluxes at states  $\beta''$  and  $\sigma''$  (along the scaled saturation vapor pressure curve,  $\ell_{f,s}$ , Figure 3) will now be introduced

$$\ell_f(T_w) = \ell_f(t) - \Delta''(t) (q_f(t) - q_f(T_w)) \quad (30)$$

Substituting  $\lambda \rho e_s(T)/(r_v p)$  for  $\ell_f$  and  $\rho c_p T/r_h$  for  $q_f$  into Eq. 30 yields

$$e_s(T_w) = e_s(t) - \Delta''(t) \gamma^*(t - T_w) \quad (31)$$

Based on the definition of the slope of a line, it can be shown that  $\Delta''(t)$  is equal to  $\Delta(t)$  (Figure 1) scaled by the reciprocal of the modified psychrometer constant

$$\Delta''(t) = \frac{\Delta(t)}{\gamma^*} \quad (32)$$

Combining Eqs. 31 and 32 yields

$$e_s(T_w) = e_s(t) - \Delta(t)(t - T_w) \quad (33)$$

Furthermore, substituting the righthand side of Eq. 33 into Eq. 29 and rearranging yields

$$e_s(t) - e_0 = \Delta(t)(t - T_w) + \gamma^*(T_0 - T_w) \quad (34)$$

Setting  $t = T_0$  and rearranging, results in

$$T_0 - T_w = \frac{e_s(T_0) - e_0}{\Delta(T_0) + \gamma^*} \quad (35)$$

Note that Eq. 35 is an exact expression, provided  $\Delta(T_0)$  is evaluated at an appropriate temperature,  $\tau$ , such that

$$\Delta(T_0) = \left. \frac{\partial e_s(T)}{\partial T} \right|_{T=\tau}, \quad \text{where } T_w \leq \tau \leq T_0 \quad (36)$$

Combining Eqs. 35 and 27 and then substituting  $\Delta_a$  for  $\Delta(T_0)$  in the resultant expression (while noting that in the adiabatic cooling process,  $\ell_{f,a} = -q_{f,a}$ ), it can be shown that the adiabatic fraction of the latent heat flux,  $\ell_{f,a}$ , can be expressed as

$$\ell_{f,a} = \rho c_p \frac{e_s(T_0) - e_0}{(\Delta_a + \gamma^*)r_h} \quad (37)$$

**2.4.3.b. Evaporation into saturated air: Diabatic heating in a state saturation accounting for the convective transfer of heat and vapor and (bulk) canopy system response**

For the diabatic component of the evaporation process, the flux form of the heat balance of the air parcel can be given as

$$Q_f = \ell_{f,d} + q_{f,d} \quad (38)$$

where  $Q_f$  is the steady external heat flux into the air parcel ( $W/m^2$ ), which is equal to the net surface heat flux minus the ground heat flux.

Considering a linear equation (of the form given in Eq. 30) that relates the point  $\beta''(T_w, e_s(T_w))$  on the scaled saturation vapor pressure curve with that of  $\zeta''(T_a, e_s(T_a))$ , i.e., a scenario in which  $\Delta''(t) = \Delta''(T_a)$ ; it can be readily observed (from Eq. 32) that  $\Delta''(T_a) = \Delta(T_a)/\gamma$ . Using  $\Delta_d$  in place of  $\Delta(T_a)$ , it follows from Figure 3 that

$$\frac{\Delta_d}{\gamma^*} = \frac{\ell_{f,d}}{q_{f,d}} \quad (39)$$

Substituting the expression  $Q_f - \ell_{f,d}$  for  $q_{f,d}$  (from Eq. 38) into Eq. 39 and rearranging yields the expression for the diabatic fraction of the latent heat flux,  $\ell_{f,d}$

$$\ell_{f,d} = \frac{\Delta_d Q_f}{\Delta_d + \gamma^*} \quad (40)$$

#### 2.4.3.c. *The Penman-Monteith system of equations*

Substituting  $\Delta$  for  $\Delta_a$  in Eq. 37 and for  $\Delta_d$  in Eq. 40 (based on the assumption  $\Delta_a \approx \Delta_d = \Delta$ , Eq. 20) and combining the resultant expressions with the equation for latent heat flux,  $\ell_f$  (Eq. 25) yields

$$\ell_f = \frac{\Delta Q_f}{\Delta + \gamma^*} + \rho c_p \frac{e_s(T_0) - e_0}{(\Delta + \gamma^*) r_h} \quad (41)$$

Following the approach used to deduce Eq. 40, the expression for the diabatic component of the sensible heat flux,  $q_{f,d}$ , can be expressed as

$$q_{f,d} = \frac{\gamma^* Q_f}{\Delta + \gamma^*} \quad (42)$$

Substituting Eq. 42 and the negative of Eq. 37 into the expression for  $q_f$  (Eq. 25) yields the equation for the net sensible heat flux into the air parcel,  $q_f$ , during evaporation

$$q_f = \frac{\gamma^* Q_f}{\Delta + \gamma^*} - \rho c_p \frac{e_s(T_0) - e_0}{(\Delta + \gamma^*) r_h} \quad (43)$$

An equation for the final temperature of the air parcel,  $T_a$ , can be deduced by combining Eq. 43 with a form of the sensible heat equation (Eq. 27), in which the temperatures corresponding to the initial and final states of the air are set to  $T_0$  and  $T_a$ , respectively.

$$T_a = T_0 + \frac{\gamma^* r_h Q_f}{\rho c_p (\Delta + \gamma^*)} - \frac{e_s(T_0) - e_0}{\Delta + \gamma^*} \quad (44)$$

It can be observed that the equation for the final air temperature, Eq. 44, is identical to the expression for the temperature of the exchange surface (e.g., Monteith and Unsworth, 2013). Considering that the surface temperature and the external heat flux into the air parcel are both held steady through the evaporation process, it can be observed that the equivalence of the expressions for the final air temperature and the surface temperature points to the fact that the surface temperature is the same as the equilibrium air temperature.

#### ***2.4.3.d. Resistance parameters***

As noted earlier, the resistance parameters to vapor and heat transfer ( $r_v$  and  $r_h$ ) are introduced into Eq. 24 to take into account the dynamic effects of turbulence generated by wind-surface interactions, and the effects of (bulk) canopy system response to atmospheric conditions, on evaporation from a field with a uniform stand of vegetation. However, the pathway for vapor transfer from a plant leaf to the atmosphere is considered to be composed of two distinct mechanisms: vapor transfer from the leaf through the stomata and cuticle to the laminar sublayer on the leaf surface by diffusion (controlled mainly by crop-physiological response to atmospheric conditions) followed by a convective vapor transport across the turbulent boundary layer (Monteith, 1965 and 1981). Thus, Monteith (1965) described the resistance to vapor

transfer,  $r_v$ , as the sum total of stomatal and cuticular resistance,  $r_s$ , and resistance to vapor transport in the turbulent boundary layer,  $r_b$  (note that partitioning of the resistance to vapor transfer along this line was also described by Penman, 1953). Accordingly, the parameter  $\gamma^*$ , Eq. 28, can be given as

$$\gamma^* = \gamma \frac{r_b + r_s}{r_h} \quad (45)$$

For an area of uniform vegetation stand,  $r_s$ , is referred to as canopy resistance (Monteith and Unsworth 2013). The equivalent parameter, in agricultural applications, is the bulk surface resistance (Allen et al. 1998), which accounts for crop-canopy system effects, including crop-physiological response to atmospheric conditions, although not limited to it. As can be noted from Eq. 45, Eqs. 41, 43, and 44 are defined in terms three different resistance parameters: the bulk surface resistance to vapor transfer,  $r_s$ , the turbulent boundary layer resistance to vapor transfer,  $r_b$ , and the resistance to heat transfer,  $r_h$ . A method for determining  $r_s$  is described by Allen et al. (1998) and Jensen and Allen (2016). Considering a neutral atmospheric condition (a widely used approximation in estimating evaporation with the Penman–Monteith equation),  $r_b$  and  $r_h$  can be considered equal, leading to the simplification

$$\gamma^* = \gamma \left( 1 + \frac{r_s}{r_a} \right) \quad (46)$$

Eq. 46 is obtained from Eq. 45 by substituting the notation  $r_a$  (s/m) for the aerodynamic resistances to vapor and heat transfer:  $r_b$  and  $r_h$ . For simplicity,  $r_a$  is often referred to as the aerodynamic resistance (e.g., Allen et al., 1998). More discussion on this along with the equation commonly used to estimate  $r_a$  in evapotranspiration estimation, in agricultural water management applications, will be presented in Chapter 3.

The equations for latent heat flux, Eq. 41, sensible heat flux, Eq. 43, and the final air temperature, Eq. 44, henceforth referred to as the Penman-Monteith system of equations, cannot be evaluated directly, because the variable  $\Delta$  is not known *a priori*. Thus, alternative numerical solutions to this system of equations are presented in Chapter 4.

## 2.5. Discussion

Approaches to the derivation of the Penman-Monteith equation can fall into two categories. The most widely used approach (e.g., Jensen and Allen, 2016; Penman, 1948) considers evaporation as vapor, heat, and momentum transfer process between a source/sink surface and a point (at measurement height) in the ambient air current. The alternative approach (Monteith, 1981), on the other hand, conceptualizes evaporation as a thermodynamic process that produces changes in the thermodynamic state of the ambient air.

Overall, the conventional approach to the derivation of the Penman-Monteith equation has the advantage of being mathematically direct and compact. The thermodynamic approach, on the other hand, is more revealing of key assumptions and concepts that are generally implicit in the conventional approach. It also brings-forth some useful physical interpretations of the terms, and mathematical attributes of key parameters, of the Penman-Monteith equation. The following describes the advantages accruing from the use of the thermodynamic formulation to the derivation of the Penman-Monteith equation and some additional points.

The thermodynamic method uses a two-step approach to derive the Penman-Monteith equation. As part of the mechanics of the derivation process, the initial step reveals that the Penman-Monteith equation is fundamentally a description of the transfer of vapor and heat between a wet

source/sink surface and a quiescent ambient air, a fact accentuated by the use of the thermodynamic equations of state to define potential difference. The dynamic effects of wind and canopy complex effects on evaporation are taken into account through the introduction of resistance parameters into the basic equations in the subsequent step. A step that underlines the notion that, in the Penman-Monteith equation, the convective transport of heat, vapor, and momentum and canopy system effects on evaporation are taken into account in the approximate sense. Although these observations can certainly be made in the context of the conventional derivation, they are, nonetheless, implicit and hence are not as obvious and natural to the derivation as is the case with the thermodynamic approach.

Another important consequence of applying the thermodynamic approach to the derivation of the Penman-Monteith equation is that it emphasizes the notion that evaporation is a process that is fundamentally driven by energy (heat) supply, although heat effects on evaporation are modulated by other weather parameters (including, vapor pressure deficit and wind speed) and crop factors. Accordingly, the thermodynamic approach shows that each term in the Penman-Monteith equation represents evaporation flux attributable to a separate heat source: (i) The sensible heat extant in the air parcel at the initial state of the air (which is a function of the thermodynamic history of the air parcel) contributes to evaporation through a process of adiabatic cooling, leading to saturation of the air at the wet-bulb temperature (Figures 1 to 3) and (ii) A steady supply of external heat (for  $T_a > T_w$ ), in the form of net surface heat flux minus the sub-medium heat flux, which contributes to a further increase in the latent heat content of the air while maintaining a state of saturation.

A close look at the conceptual charts (Figures 1 to 3) used in the derivation presented here, in light of the fact that the final (equilibrium) air temperature is equal to the steady surface temperature, readily reveals that evaporation can occur with a surface temperature that is less than the air temperature, provided the surface temperature is greater than the dewpoint temperature. While such an observation can possibly be made in the context of the conventional derivation, it would, however, be intuitive and hence not as evident and inherent to the derivation as is the case with the thermodynamic approach.

Given that the thermodynamic derivation is based on conceptual charts depicting the energy states of the air parcel (Figures 1 to 3), it readily reveals the mathematical/physical attributes of a key parameter of the Penman-Monteith equation,  $\Delta$  (i.e., the slope of a line connecting a pair of points on the saturation vapor pressure curve). Specifically, the thermodynamic formulation readily reveals that the introduction of the  $\Delta$  parameter allowed for any thermodynamic state on the saturation vapor pressure curve,  $[t, e_s(t)]$  in Figure 1, to be related to that of  $[T_w, e_s(T_w)]$  with a simple, yet exact (linear) equation, provided  $\Delta$  is allowed to vary with the air temperature,  $t$ . The derivation has led to an alternative form of the Penman-Monteith equation, which is expressed in terms of  $\Delta_a$  and  $\Delta_d$  (shorthand for  $\Delta(T_0)$  and  $\Delta(T_a)$ , respectively). However, in the interest of keeping the resultant equation simple  $\Delta$  is treated as a constant (i.e.,  $\Delta_a \approx \Delta_d$ ), contingent on the assumption that the temperature interval  $[T_0, T_a]$  is sufficiently small for the accuracy of the resultant expression to be considered acceptable. Note that this concept is key to the derivation of the Penman-Monteith equation.

The derivation shows that the introduction of the air density parameter into the thermodynamic equations of state and hence into the Penman-Monteith equation, which resulted in heat contents of the air being expressed in a unit volume basis, presumes that the range of (air) temperature variation during evaporation, i.e.,  $[T_a - T_w]$ , is sufficiently small for the density of the air to be adequately represented by an average value. Note that this constraint on the range of temperature variation is independent of the requirement that relates to the constancy assumption of the  $\Delta$  parameter.

A close look at the Penman-Monteith equation shows that both terms of the equation contain the modified psychrometer constant,  $\gamma^*$ , which is a function of the aerodynamic resistance parameter. The fact that both terms of the Penman-Monteith equation represent thermal energy flux, only from different sources, and that both terms contain the parameter  $\gamma^*$  suggest that the thermodynamic description of the terms as adiabatic and diabatic components (Monteith and Unsworth, 2013) might be a more precise interpretation.

In the conventional approach to the derivation of the Penman-Monteith equation, potential difference is defined as the difference in energy levels between two points in space (i.e., a point in the source/sink surface and another one in the air current). By contrast, in the thermodynamic formulation, potential difference is defined as the difference in the energy levels between the thermodynamic states of a suitably defined system. Thus, this may raise the question whether the physical meaning associated with the parameters  $r_v$  and  $r_h$  in the conventional approach (as resistance parameters to the transfer of vapor and heat, respectively) and the method used to

evaluate them can apply to the thermodynamic formulation. This point may, perhaps, need to be looked into in some detail in a follow up study.

## **Chapter 3. Integrated forms of the vapor, heat, and momentum transfer equations and the respective resistance parameters**

### **3.1. Introduction**

Natural evaporation from a field with a uniform stand of vegetation is generally modelled as a process involving the transfer of vapor and heat between an exchange surface and the ambient air. The surface being a virtual plane, within the vegetation canopy, that serves as an effective source/sink for the physical constituents of interest. The transport mechanism consists of a near surface turbulent transport process, which is coupled to the canopy system response to atmospheric conditions. While the turbulent transport processes are attributed to forced convection produced by wind-surface interactions (in practice, by wind and canopy system interactions), the (bulk) canopy system response to atmospheric conditions, on the other hand, include crop physiological response to atmospheric conditions, although not limited to it.

As shown in Chapter 2, the Penman-Monteith system of equations takes into account the convective transfer of constituents across the turbulent boundary layer and bulk canopy system effects, in an approximate manner, through the introduction of resistance parameters to the equations of state, Eqs.1 and 2. This chapter presents equations for the resistance parameters.

While the focus in evaporation studies is, mainly, on vapor and heat transport, the transfer of momentum is also inextricably coupled to the evaporation process. Thus, following Monteith (1981) and Monteith and Unsworth (2013), relationships between fluxes and potential gradients are used here to obtain integral expressions for the resistance parameters to vapor,

sensible heat, and momentum transfer. It is shown that, under neutral atmospheric conditions, the (aerodynamic) resistance to vapor and heat transfer are equal, but are greater than the aerodynamic resistance to momentum transfer. Furthermore, the expression for the aerodynamic resistance to momentum transfer (which relates the resistance parameter to the average horizontal wind velocity at measurement height, wind measurement height from the ground surface, and surface roughness and form factor - both of which are dependent on crop characteristics) is derived. An expression that relates the aerodynamic resistance to momentum with those of vapor/heat transfer is reviewed. The chapter then closes by presenting the equation widely used to evaluate the aerodynamic resistance to vapor/heat transfer and with a reference to a method for estimating the bulk surface resistance in agricultural water management applications (Allen et al., 1998).

### **3.2. Integrated forms of the transfer equations**

The steady-state vertical flux of vapor, heat, or momentum in the ambient air, where molecular processes dominate, can be expressed as the product of a transfer coefficient, the density of air, and the spatial gradient of the physical constituent of interest. These equations are based on Fick's law for diffusive transport of vapor, Fourier's equation for heat conduction, and Newton's law of viscosity for momentum. Equations of the same form are used to model the convective transfer of each of these physical quantities but with a different set of transfer coefficients (Monteith and Unsworth, 2013). Thus, the expression for vapor, sensible heat, and momentum flux across a transport pathway can be given as

$$F_v(z) = -\rho(z)K_v(z)\frac{d\xi}{dz} \quad (1)$$

$$F_h(z) = -\rho(z)K_h(z)\frac{d(c_p T)}{dz} \quad (2)$$

$$F_m(z) = \rho(z)K_m(z)\frac{du}{dz} \quad (3)$$

In Eqs. 1 to 3,  $F_v$  is vapor flux (kg/s-m<sup>2</sup>);  $F_h$  is sensible heat flux (W/m<sup>2</sup>), and  $F_m$  is momentum flux (N/m<sup>2</sup>);  $\rho$  is the density of air (kg/m<sup>3</sup>);  $K_v$ ,  $K_h$ , and  $K_m$  are the turbulent transfer coefficient for vapor, heat, and momentum, respectively (m<sup>2</sup>/s); and  $u$  is time averaged horizontal wind velocity (m/s); and  $z$  (m) vertical distance referenced from the ground surface. Note that in Eqs. 1 to 3, the parameters  $F_v$ ,  $F_h$ ,  $F_m$ ,  $\rho$ ,  $K_v$ ,  $K_h$ ,  $K_m$ ,  $\xi$ ,  $T$ , and  $u$  are parameters expressed as functions of above ground height.

Now, consider the transfer of the physical constituents across a pair of points, labeled here as points 1 and 2, subject to the following simplifying assumptions: (i) flux,  $F$ , is constant across the points. And (ii) the scale of the transfer pathway is such that the variation in air density,  $\rho(z)$ , can be considered sufficiently small and hence it can be represented adequately by an average value,  $\rho$  (Monteith, 1981). The constant fluxes of the physical quantities can then be evaluated based on the integrated forms of Eqs. 1 to 3. A general form of the flux integral expression describing the convective transfer of vapor, sensible heat, and momentum can be expressed as

$$F = \text{sign}(\delta\pi) \rho \frac{\pi_2 - \pi_1}{\int_{z_1}^{z_2} \frac{dz}{K(z)}} \quad (4)$$

In Eq. 4,  $F$  is the constant flux of a constituent (which could be vapor, sensible heat, or momentum) across the transfer pathway,  $\delta\pi$  is  $\pi_2 - \pi_1$ , and  $\pi_1$  and  $\pi_2$  are the quantity of a given physical constituent in a unit mass of air at points 1 and 2, respectively. Note that if the physical constituent to be evaluated in Eq. 4 is vapor flux, then  $\pi$  represents the specific humidity of the

air,  $\xi$ , and  $K$  represents  $K_v$ . If, on the other hand, the constituent of interest is sensible heat, then  $\pi$  stands for the product  $c_p T$  and  $K$  represents  $K_h$ . For the case in which the constituent of interest is momentum,  $\pi$  represent the time averaged horizontal velocity of wind,  $u$ , and  $K$  represents  $K_m$ . Observe that the introduction of the signum function allows Eq. 4 to be consistent with Eqs. 1 to 3.

Taking a close look at Eq. 4, one may draw analogy between Ohm's law which relates the current (flux of electrical charge) between two points in a circuit with the quotient of the electrical potential difference between the points and the resistance across the points. Accordingly, the numerator on the righthand side of Eq. 4 can be viewed as the potential difference between points 1 and 2 and the denominator can be considered as the resistance to the transfer of a physical constituent across the transfer pathway, which can be expressed as

$$F = \text{sign}(\delta\pi) \frac{\rho \delta\pi}{r} \quad (5)$$

In Eq. 5,  $r$  (s/m) is the resistance to the turbulent transfer of a constituent between the points. Based on Eqs. 4 and 5, the aerodynamic resistance parameter,  $r$ , can now be expressed as

$$r = \int_{z_1}^{z_2} \frac{dz}{K(z)} \quad (6)$$

Considering an atmospheric condition in neutral stability (a common practice in estimating evaporation), momentum, heat, and vapor are considered to be transported equally effectively (Monteith and Unsworth, 2013). In other words, under a unit potential gradient the flux of each of these quantities must be equal. Thus, based on Eqs. 1 to 3 and the simplifying assumptions that led to Eq. 4, it can be observed that the transfer coefficients for vapor, heat, and momentum are equal

$$K_m = K_h = K_b \quad (7)$$

Equation 7 coupled with Eq. 6 can be used to deduce an important relationship between the aerodynamic resistance parameters for heat, vapor, and momentum. Given the relationship in Eq. 7, it can be observed that the aerodynamic resistance parameters for heat, vapor, and momentum would be the same if the intervals of integration in Eq. 6 are the same for all the physical constituents of interest. The transfer pathway of the respective constituents is generally limited by the source/sink surfaces and the height at which wind velocity, vapor pressure, and temperature are measured in the ambient air current.

While the apparent source/sink surface for vapor and heat is the same, the apparent sink for momentum is located at a higher level in the canopy (Monteith and Unsworth, 2013). Now, if we assume the measurement height for vapor pressure and temperature are the same, it can then be observed based on the relationships given in Eq. 6 and 7 that the resistance to the turbulent transfer of vapor,  $r_b$ , and that of heat,  $r_h$ , can be considered the same.

$$r_b = r_h \quad (8)$$

The resistance to the turbulent transfer of momentum, however, is smaller than  $r_b$  and  $r_h$ .

Accordingly, the expression for the modified psychrometer constant,  $\gamma^*$ , (Eq. 45 of Chapter 2) can be simplified to

$$\gamma^* = \gamma \left( 1 + \frac{r_s}{r_a} \right) \quad (9)$$

Note that Eq. 9 is obtained from Eq. 45 (Chapter 2) by setting  $r_a = r_b = r_h$ . The notation  $r_a$  is the aerodynamic resistance to vapor and heat transfer and is often referred to, simply, as the aerodynamic resistance.

The bulk surface resistance,  $r_s$ , can be evaluated as a function of stomatal resistance and crop leaf area index with a method described by Allen et al. (1998) and Allen (1986). An equation widely used to evaluate the aerodynamic resistance,  $r_a$ , in agricultural water management applications will be presented later in the chapter. Before that, however, an expression will be derived for the resistance to momentum transfer,  $r_m$ , and the relationship between  $r_m$  and  $r_a$  will be explored.

### 3.3. Aerodynamic resistances to momentum, vapor, and heat transfer

#### 3.3.1. Logarithmic wind velocity profile

The vertical profile of the time averaged horizontal wind velocity, which can be the local momentum in a unit mass of air, is a key input in the development of expressions for the aerodynamic resistance parameters for vapor, heat, and momentum. Thus, first, an expression will be derived for the wind velocity profile. To start the derivation, consider the equation for the shearing stress,  $\tau$  (N/m<sup>2</sup>), that wind exerts on the surface that constitutes the apparent sink for momentum

$$\tau = \rho K_m(x) \frac{du}{dz} \quad (10)$$

where  $x$  is the vertical distance referenced from the surface that serves as the sink for momentum. Note that the shear stress,  $\tau$ , is the same as momentum flux  $F_m(z)$ , given in Eq. 3.

Equation 10 can be expressed as

$$\frac{du}{dz} = \frac{\tau}{\rho K_m(x)} \quad (11)$$

A mathematically equivalent form to Eq. 11 is

$$\frac{du}{dz} = f(\tau, \rho, x) \quad (12)$$

An alternative expression for the velocity gradient can be deduced based on dimensional reasoning (e.g., Arya, 1991). Thus, following Buckingham's  $\pi$  theorem it can be shown that

$$\frac{du}{dz} = \frac{\nu}{x} \sqrt{\frac{\tau}{\rho}} \quad (13)$$

In Eq. 13,  $\nu$  is a dimensionless proportionality constant [-] and is taken to be the reciprocal of a physical constant called the von Karman constant ( $\kappa$ ), and the expression  $\sqrt{\frac{\tau}{\rho}}$  is the shear velocity,  $u_*$  (m/s).

Eq. 13 can, now, be expressed in terms of the shear velocity,  $u_*$ , as follows

$$\frac{du}{dz} = \frac{u_*^2}{\kappa u_* x} \quad (14)$$

Furthermore, Eq. 11 can be written in terms of  $u_*$  as

$$\frac{du}{dz} = \frac{u_*^2}{K_m(x)} \quad (15)$$

It can be observed from Eqs. 14 and 15 that

$$K_m(x) = \kappa u_* x \quad (16)$$

For fields with vegetation, the ground surface is not the effective sink for momentum. Instead, it is a plane somewhere above the ground but within the crop canopy. The above ground height of this surface is termed as the zero-plane displacement,  $d$ . Thus, for vegetated fields, the variable,

$x$ , in Eq. 16 can be given as  $x = z-d$ . Substituting the expression  $z-d$  for  $x$  into Eq. 16, then combining Eqs. 16 with 15, and rearranging yields

$$du = \frac{u_*}{\kappa(z-d)} dz \quad (17)$$

Integrating the lefthand side of Eq. 17 between  $u = 0$  and  $u = u(Z)$ , (i.e., the average wind velocity at height  $Z$ ) and the righthand side between a lower limit of  $d+z_{0m}$  (i.e., the height at which  $u = 0$ ) and an upper limit of  $Z$ , yields an expression for  $u(Z)$

$$u(Z) = \frac{u_*}{\kappa} \ln \left( \frac{Z-d}{z_{0m}} \right) \quad (18)$$

In Eq. 18,  $z_{0m}$  (m) is a constant termed as the roughness length for momentum transfer. Penman and Long (1959) reported that a logarithmic wind profile of the form given in Eq. 18 conforms to experience under neutral atmosphere. For atmospheric conditions that are not neutral, the righthand side of Eq. 18 need to be augmented with an additional term (e.g., Jensen and Allen, 2016). Note that  $d+z_{0m}$  is the above ground height of the surface that serves as the apparent sink for momentum (i.e., the height at which the theoretical logarithmic wind velocity profile is zero).

### ***3.3.2. Equation for the resistance to momentum transfer, $r_m$***

Following Monteith and Unsworth (2013), the derivation of the expression for the aerodynamic resistance to momentum transfer,  $r_m$ , starts with a statement of the shearing stress equation.

$$\tau = \rho K_m \frac{du}{dz} \quad (19)$$

Based on Ohm's law analogy (Eq. 4), Eq. 19 can be expressed as the ratio of the difference between the momentum in a unit volume of air at points 2 and 1 and the resistance to momentum transfer between the points

$$\tau = \rho \frac{u_2 - u_1}{r_m} \quad (20)$$

Noting that  $u_*^2 = \frac{\tau}{\rho}$ , and rearranging terms yields an expression for the aerodynamic resistance

$$r_m = \frac{u_2 - u_1}{u_*^2} \quad (21)$$

For a scenario in which wind velocity is measured at two points, i.e.,  $Z_1$  and  $Z_2$ , the expression for  $r_m$  can be obtained by substituting the expressions for  $u_2$  and  $u_1$  (Eq. 18) into Eq. 21

$$r_m = \frac{\frac{u_*}{k} \left( \ln \left( \frac{Z_2 - d}{z_{0m}} \right) - \ln \left( \frac{Z_1 - d}{z_{0m}} \right) \right)}{u_*^2} = \frac{\ln \left( \frac{Z_2 - d}{Z_1 - d} \right)}{k u_*} \quad (22)$$

If, on the other hand, wind speed is measured at a single point, say at height  $Z$  (as is commonly the case in practice), then the other point on the wind velocity profile can be assumed to be at the height where  $u = 0$  (i.e.,  $d + z_{0m}$ ). Equation 21 can, thus, be expressed as

$$r_m = \frac{u(Z) - u(d + z_{0m})}{u_*^2} \quad (23)$$

Substituting the expression for  $u(Z)$ , from Eq. 18, into Eq. 23 and noting that  $u(d + z_{0m}) = 0$  yields

$$r_m = \frac{\ln \left( \frac{Z - d}{z_{0m}} \right)}{k u_*} \quad (24)$$

Substituting the expression for  $u_*$ , from Eq. 18, into Eq. 24 and simplifying results in the expression for the aerodynamic resistance to momentum

$$r_m = \frac{\ln\left(\frac{Z-d}{z_{0m}}\right)^2}{k^2 u(Z)} \quad (25)$$

### 3.3.3. Equation for the aerodynamic resistance parameters, $r_a$

Monteith and Unsworth (2013), expressed  $r_a$  in a form analogous to that of  $r_m$ , Eq. 24, as follows

$$r_a = \frac{\ln\left(\frac{Z-d}{z_{oh}}\right)}{k u_*} \quad (26)$$

where  $z_{oh}$  is the roughness length for heat and vapor transfer. Given that  $r_a > r_m$ , it can be observed that  $z_{oh} < z_{0m}$ . Noting that the righthand of Eq. 26 can be expressed as

$$r_a = \frac{\ln\left(\frac{Z-d}{z_{0m}}\right)}{k u_*} + \frac{\ln\left(\frac{z_{0m}}{z_{oh}}\right)}{k u_*} \quad (27)$$

It can be observed that  $r_a$  is the sum of the aerodynamic resistance to momentum,  $r_m$ , (Eq. 24) and a term defined as a function of the ratio of  $z_{0m}$  to  $z_{oh}$ .

Equation 27 is significant for its conceptual value. However, the equation widely used in the evaluation of the aerodynamic resistance in agricultural water management applications is the form given by Allen et al. (1998), which is also described by Brutsaert (1982).

$$r_a = \frac{\ln\left(\frac{Z_m-d}{z_{0m}}\right) \ln\left(\frac{Z_h-d}{z_{oh}}\right)}{k^2 u(Z)} \quad (28)$$

In Eq. 28,  $Z_m$  and  $Z_h$  are measurement heights for wind and vapor pressure (m), respectively;  $z_{0m}$  is the roughness length for momentum transfer (m); and  $z_{oh}$  is the roughness length for heat and vapor transfer (m). Note that Eq. 28 is of analogous form as Eq. 25.

An important note here is that in the conventional approach to the derivation of the Penman-Monteith equation, potential difference is defined as the difference in energy levels between two points in space (i.e., a point in the source/sink surface and another one in the air current). By contrast, in the thermodynamic formulation (Chapter 2), potential difference is defined as the difference in the energy levels between the thermodynamic states of a suitably defined system. Thus, this may lead to the question whether the physical meaning associated with the parameters,  $r_v$  and  $r_h$  (Eq. 24 of Chapter 2), in the conventional approach (as resistance parameters to the transfer of vapor and heat, respectively) and the method used to evaluate them can apply to the thermodynamic formulation. This point may, perhaps, need to be looked into in some detail in a follow up study.

## **Chapter 4. The Penman-Monteith system of equations: Numerical solutions and evaluation**

### **4.1. Introduction**

A review of the derivation of the Penman-Monteith equation based on the thermodynamic approach of Monteith (1965; 1981) is presented in Chapter 2. Description of the development and evaluation of numerical solutions to the resultant set of equations is the subject of this chapter.

From an agricultural water management standpoint, the most important equation that emerges from the derivation is the expression for latent heat flux,  $\ell_f$ . However, in its basic form, the Penman–Monteith equation is not an explicit formula for  $\ell_f$ , because the slope parameter related

to the saturation vapor pressure curve,  $\Delta$ , is not a given parameter, it is instead a variable. As a result, the  $\ell_f$  equation along with the sensible heat,  $q_f$ , and the final air temperature,  $T_a$ , equations represent a coupled set of three equations in four variables ( $\ell_f$ ,  $q_f$ ,  $T_a$ , and  $\Delta$ ). Evidently, this system of equations is in indeterminate form.

One of two approaches can be used to circumvent this problem. The most widely used approach, referred here as the conventional model, determines  $\Delta$  independently, based on the assumption that a satisfactory approximation of  $\Delta$  can be obtained if it is set to the slope of the saturation vapor pressure curve at the measured air temperature,  $T_0$  (Allen et al., 1998; Jensen and Allen, 2016; Howell and Evett, 2004). Substituting the  $\Delta$  value obtained as such into the  $\ell_f$ ,  $q_f$ , and  $T_a$  equations leads to an uncoupled set that can be solved directly. This simplification is equivalent to local linearization of the saturation vapor pressure function about  $T_0$ . While it is advantageous in the sense that it leads to an uncoupled system of equations that can be solved directly, it, nonetheless, introduces a level of approximation in the variable estimates (Paw U and Gao, 1988).

An alternative approach (e.g., McArthur 1990, 1992) involves augmenting the  $\ell_f$ ,  $q_f$ , and  $T_a$  equations with an approximate expression that is obtained based on the constancy assumption of  $\Delta$  described in Chapter 2 [Note: for brevity, this equation will henceforth be referred to as the  $\Delta$  equation]. The resultant set consisting of four equations in four variables ( $\ell_f$ ,  $q_f$ ,  $T_a$ , and  $\Delta$ ) can then be solved numerically.

A different set of solutions that compute the latent heat and sensible heat fluxes along with the surface temperature iteratively exist (e.g., Bristow 1987; Lascano and van Bevel 2007). In general, these approaches combine the basic energy flux ( $\ell_f$  and  $q_f$ ) equations with the surface

energy balance equation leading to a form expressed in terms of the surface temperature, which is then solved with a suitable iterative method. Although these formulations are based on the same basic physical principles as that of the Penman–Monteith equations, they, nonetheless, differ from the Penman–Monteith form and hence were not considered in the current study.

In the study reported here, four alternative algorithms (labeled as model 1, 2, 3, and 4) were developed and evaluated: *Model 1* consists of a programmatic implementation of McArthur’s approach, which uses a sequential function-evaluation based iterative solution of the final air temperature,  $T_a$ , and the  $\Delta$  equations. *Model 2* is based on a simultaneous iterative solution of the  $T_a$  and  $\Delta$  equations. *Model 3* uses Newton iteration of a nonlinear equation in  $T_a$ , obtained by combining the  $T_a$  and  $\Delta$  equations in a way that eliminates  $\Delta$ . And *Model 4* involves a simultaneous iterative solution of a variant of the complete set of equations obtained by recasting each of the latent heat flux, sensible heat flux, and the final air temperature equations into a form where the variables are  $\ell_f$ ,  $q_f$ , and  $T_a$  only.

Model 1, 2, or 3 uses a two-step approach to compute the evaporation variables. First, the  $T_a$  and  $\Delta$  values or the  $T_a$  value, as the case may be, is computed (based on a suitable iterative method) and in a second step, the resultant  $\Delta$  is substituted in the latent heat and sensible heat equations to determine  $\ell_f$  and  $q_f$ . On the other hand, model 4 computes the variables through simultaneous iterative solution. While model 4 should in principle lead to an accurate solution, the inclusion of models 1, 2, and 3 in the current study was justified on the consideration that they may potentially represent simpler and sufficiently accurate alternative to model 4.

To the best of the current authors’ knowledge, the study by McArthur (1990) is the only published work that solved the Penman-Monteith equations iteratively, thus, the results of

McArthur were considered in the current study as reference solution. Accordingly, the alternative models developed in the current study were evaluated through comparison of model outputs with McArthur's data. Results of model verification showed that each of the alternative models produced outputs that are essentially identical and also in close agreement with the reference solution. The mean absolute residuals between variable estimates computed with the models presented here and those reported by McArthur range from a minimum of about 0.2% for  $T_a$  and a maximum of 1.9% for  $\Delta$ . Furthermore, intercomparison of the alternative models based on the criteria of numerical efficiency and robustness revealed that each model represents a comparable alternative, to each of the other models, for estimating evaporation. However, model 1 (which is based on sequential function-evaluation approach) is simpler than the other models (which are based on a simultaneous iterative solution of the complete set or reduced form thereof) both conceptually and in terms of its numerical formulation and programmatic implementation. Thus, model 1 was considered for further analysis.

The performance of model 1 is then compared to that of the conventional model based on a total of seven hypothetical data sets, covering a wide range of natural evaporation conditions. The results suggest that differences in the methods used for estimating  $\Delta$  have the maximum effect on sensible heat flux estimates (where the mean absolute residual is 18.1%), a negligible effect on estimates of the final air temperature (with an average residual of 0.7%), and a limited effect on the estimates of latent heat flux (where the mean residual is 8.2%).

Given that both model 1 and the conventional model involve a level of approximation in the determination of  $\Delta$ , it can be observed that direct comparison of the two models cannot provide answer to the question: which model is more accurate? Thus, the current study does not answer that question. However, considering the latent heat flux,  $\ell_f$  (which is the most important

of the evaporation variables as far as irrigation management applications are concerned), the relatively small average residual (of 8.2%) suggests that differences between  $\ell_f$  estimates obtained with model 1 and the conventional model should typically be within the margin of error of the conventional model. This observation suggests that, typically, the use of both the conventional model and model 1 can be considered equally acceptable from the standpoint of accuracy.

## 4.2. Outline of the chapter

A brief review of the Penman-Monteith system of equations is summarized in a section titled theory, which is then followed by a description of numerical solutions, consisting of four of alternative algorithms. Evaluation of the performance of the alternative numerical solutions based on comparison of model outputs with the results reported by McArthur (1990) is presented in a subsequent segment. Intercomparison of the alternative models and model selection, for further consideration, is described next. In the last section of the chapter, a comparison of the selected model with the conventional model (i.e., the approach widely used to evaluate the Penman-Monteith set of equations) is presented, followed by description and analysis of the output data and a discussion on implications of results on the relative accuracy of the models.

## 4.3. Theory

The Penman-Monteith system of equations, derived in the companion manuscript, are summarized here for convenience

$$\ell_f = \frac{\Delta Q_f}{\Delta + \gamma^*} + \rho c_p \frac{e_s(T_0) - e_0}{(\Delta + \gamma^*)r_a}, \quad \text{where } \ell_f = \lambda E \text{ and } \gamma^* = \gamma \left(1 + \frac{r_s}{r_a}\right) \quad (1)$$

$$q_f = \frac{\gamma^* Q_f}{\Delta + \gamma^*} - \rho c_p \frac{e_s(T_0) - e_0}{(\Delta + \gamma^*) r_a} \quad (2)$$

$$T_a = T_0 + \frac{\gamma^* r_a Q_f}{\rho c_p (\Delta + \gamma^*)} - \frac{e_s(T_0) - e_0}{\Delta + \gamma^*} \quad (3)$$

In Eqs. 1 to 3,  $\ell_f$  (W/m<sup>2</sup>) is latent heat flux;  $\lambda$  (J/Kg) is the latent heat of vaporization of water;  $E$  (Kg/s-m<sup>2</sup>) is evaporation flux;  $\Delta$  (KPa/K) is slope parameter related to the saturation vapor pressure function;  $Q_f$  (W/m<sup>2</sup>) is the available energy for partitioning into sensible and latent heat components (i.e., the external heat flux into the air, which is equal to the net surface heat flux minus the sub-medium heat flux);  $\gamma^*$  (KPa/K) is the modified psychrometer constant;  $\gamma$  (KPa/K) is the psychrometer constant;  $r_s$  (s/m) is bulk surface resistance;  $r_a$  (s/m) aerodynamic resistance;  $\rho$  (Kg/m<sup>3</sup>) is the density of the ambient air;  $c_p$  (J/Kg-K) is the heat capacity of the air at constant pressure;  $e_s(T)$  (KPa) is the saturation vapor pressure at temperature,  $T$ ;  $T_0$  (K) is the measured air temperature;  $e_0$  (KPa) is the measured vapor pressure; and  $T_a$  (K) is the final air temperature.

In Eqs. 1 to 3, the latent heat flux,  $\ell_f$ , the slope parameter related the saturation vapor pressure curve,  $\Delta$ , the sensible heat flux,  $q_f$ , and the final air temperature,  $T_a$ , are variables and the rest of the physical quantities are given parameters. Notably, this system of equations contains three equations with four variables, which implies that it is of indeterminate form. Thus, in order to obtain a unique solution, the system must be conditioned following either one of the following approaches: one of the variables needs to be determined independently of Eqs. 1 to 3 or Eqs. 1 to 3 need to be augmented with an additional equation. Generally, the following two approaches are used to solve this problem, both involving a level of approximation in the determination of  $\Delta$ .

The most widely used approach, referred here as the conventional model, assumes that a satisfactory approximation of  $\Delta$  can be obtained if it is set to the slope of the saturation vapor pressure function at the measured air temperature,  $\left. \frac{de_s}{dT} \right|_{T=T_0}$ , (Allen et al., 1998; Jensen and Allen, 2016; Howell and Evett, 2004). The assumption is predicated on the consideration that the difference between the surface and the air temperatures are generally sufficiently small for  $\left. \frac{de_s}{dT} \right|_{T=T_0}$  to be a good approximation of  $\Delta$  and for the resultant estimate of  $\ell_f$  to be of acceptable accuracy. The  $\Delta$  value determined, as such, can then be substituted into Eqs. 1–3 to calculate  $\ell_f$ ,  $q_f$ , and  $T_a$  directly. The fact that the approach leads to an uncoupled set of equations is an advantage, but this simplification leads to an approximation error.

The second approach involves augmenting Eqs. 1 to 3 with an additional equation of the form

$$e_s(T_0) = e_s(T_a) - \Delta(T_a - T_0) \quad (4)$$

Note that Eq. 4 is an approximate expression deduced from Eq. 12 of Chapter 2 based on the constancy assumption of  $\Delta$  (McArthur 1990). The exact form of Eq. 12 (in Chapter 2) requires  $\Delta$  to vary with the air temperature, which would have resulted in a pair of equations, wherein one of the equations is expressed in terms of  $\Delta_a = \Delta(T_0)$  and another one given in terms of  $\Delta_d = \Delta(T_a)$  [note that  $\Delta_a$  and  $\Delta_d$  are the exact values of the parameter associated with the adiabatic and diabatic components]. However, if the difference between the measured and final air temperatures,  $[T_0, T_a]$ , encountered in a natural evaporation process can be considered sufficiently small, then  $\Delta$  can be treated as a constant (e.g., Monteith 1981), which leads to the relationship given in Eq. (4). Given Eq. 4, it can be observed that the resultant set, consisting of

Eqs. 1–4, represents a system of four equations in four variables ( $\ell_f$ ,  $q_f$ ,  $T_a$ , and  $\Delta$ ) for which iterative solutions can be readily developed based on standard iteration methods. Considering that Eq. 4 is not an exact expression, it ought be noted here that the iterative approach (wherein  $\Delta$  is assumed constant) also involves a level of approximation.

A simultaneous solution of the complete set of equations (Eqs. 1 to 4 or modified forms thereof) should in principle lead to a more accurate solution. However, a close look at Eqs. 1 and 2 reveals that these equations contain one variable each ( $\ell_f$  in the case of Eq. 1 and  $q_f$  in the case of Eq. 2) that do not appear in any of the other equations (i.e., Eqs. 3 and 4). Furthermore, Eqs. 1 and 2 share only the variable  $\Delta$  with the other equations. This observation suggests that in their current form, Eqs. 1 and 2 are not as strongly coupled to Eqs 3 and 4, as for instance Eq. 3 is to that of Eq. 4 or vice-versa (where both equations are functions of  $T_a$  and  $\Delta$ ). The preceding observation suggests that a simpler formulation, than a simultaneous solution of the complete set of equations, could lead to sufficiently accurate but more efficient and robust solutions. More discussion on this will be provided in Section 4.6.4.

Accordingly, in the current development alternative solution techniques with a varying degree of complexity were developed and evaluated: (i) Programmatic implementation of McArthur’s sequential function-evaluation based iterative scheme, in which Eqs. 3 and 4 are first solved for  $T_a$  and  $\Delta$  and then the  $\Delta$  value obtained as such is substituted into Eqs. 1 and 2 to determine  $\ell_f$  and  $q_f$  (referred here as model 1). (ii) Simultaneous iterative solution of Eqs. 3 and 4 for  $T_a$  and  $\Delta$  with the Newton method, followed by calculation of  $\ell_f$  and  $q_f$  with Eqs. 1 and 2 (labeled as model 2). (iii) Newton iteration of a nonlinear equation in  $T_a$ , obtained by combining Eqs. 3 and 4 in a way that eliminates  $\Delta$ . The  $T_a$  value computed as such is then substituted in Eq. 4 to determine  $\Delta$ , which in turn is substituted into Eqs. 1 and 2 to calculate  $\ell_f$  and  $q_f$  (described as

model 3). And (iv) Simultaneous iterative solution of a form of the complete set of equations obtained by recasting Eqs. 1 to 3 into a form where the variables are  $\ell_f$ ,  $q_f$ , and  $T_a$  only (referred here as model 4).

#### **4.4. Numerical solution**

Alternative numerical solutions, described here as models 1, 2, 3, and 4, were developed for the system of equations presented earlier. Models 1, 2, and 3 use a two-step approach to determine the variables:  $\ell_f$ ,  $q_f$ ,  $T_a$ , and  $\Delta$ . The first phase uses different formulations/iteration methods to solve Eqs. 3 and 4 for  $T_a$  and  $\Delta$ . Then, in the second phase, the  $\Delta$  value so computed is substituted into Eqs. 1 and 2 to determine  $\ell_f$  and  $q_f$ , respectively. Model 4, on the other hand, computes the variables  $\ell_f$ ,  $q_f$ , and  $T_a$  through a simultaneous solution of a form Eqs. 1 to 4. A description of the equations and outlines of the numerical algorithms are presented here.

##### **4.4.1. Function evaluation based iterative scheme of McArthur (1990), model 1**

###### **4.4.1.a. Model description**

Model 1 consists of an algorithm for the programmatic implementation of McArthur's approach to the solution of Eqs. 1 to 4. With this approach, Eqs. 3 and 4 are decoupled from Eqs. 1 and 2 and are solved for  $\Delta$  and the surface temperature,  $T_s$ . As noted in Chapter 2, the variable referred to as the final (equilibrium) air temperature,  $T_a$ , in the current formulation is in fact the surface temperature. Thus, for consistency,  $T_a$  will be used in place of  $T_s$  in this manuscript.

With the sequential function-evaluation based approach of McArthur, iteration starts by setting the initial estimate of  $\Delta$  to the slope of the saturation vapor pressure function at the measured air temperature,  $T_0$ . The initial value of  $\Delta$  is then substituted into Eq. 3 to calculate the corresponding value of the final air temperature,  $T_a$ . The  $T_a$  value determined as such is then substituted into Eq. 4 to obtain a revised estimate of  $\Delta$ , which in turn is used to calculate a revised estimate of  $T_a$  with Eq. 3. In each iteration, two function evaluations are performed sequentially leading to revised estimates of the variables  $\Delta$  and  $T_a$ . At the end of each iteration, the latent heat flux,  $\ell_f$ , is calculated as a function of the current value of  $\Delta$  and then convergence test is conducted. Convergence is assumed when the incremental changes in  $\Delta$ ,  $T_a$ , and  $\ell_f$  in an iteration are considered sufficiently small.

For convenience, a pair of modifications are introduced (to McArthur's approach) in the development and implementation of the algorithm for model 1. Unlike McArthur's solution, in the current algorithm latent heat flux,  $\ell_f$ , is not calculated at every iteration. Instead, it is computed only once based on the  $\Delta$  value obtained at convergence. The reason is explained as follows. A close look at the equations for  $\ell_f$ ,  $T_a$ , and  $\Delta$  shows that, in any given iteration,  $\ell_f$  is evaluated as a function of the current value of  $\Delta$ . However, the latent heat flux,  $\ell_f$ , obtained as such cannot be substituted back into Eqs. 3 and 4 where it can affect the  $\Delta$  and  $T_a$  values computed in subsequent iterations. In other words,  $\ell_f$  calculated in a given iteration does not contribute to improvements in the solution in subsequent iterations, thus, it need not be evaluated in any of the iterations, except the last.

Furthermore, in model 1, the iterative solution is initiated with the final air temperature,  $T_a$ , set to  $1.05T_0$ . By contrast, McArthur's solution (as noted earlier) begins by setting  $\Delta$  to

$\left. \frac{de_s}{dT} \right|_{T=T_0}$ . As a result, in the algorithm presented here, the sequence of function evaluations (in an iteration) takes place in reverse order compared to that of McArthur's approach. Note that starting the iteration by initializing the final air temperature, instead of that of  $\Delta$ , was considered here a more intuitive and convenient option. Nevertheless, the two approaches are substantively the same and it can be shown that they produce the same results.

### ***Computational procedure, model 1***

1. Initialize the iteration index and variables:

(1a) Set the iteration index,  $i$ , to 0. Go to step 1b.

(1b) Set  $T_a^i = 1.05T_0$ , where  $T_a^i$  is the  $i$ th estimate of  $T_a$ . Go to step 2.

2. Calculate the  $i$ th estimate of  $\Delta$ ,  $\Delta^i$ , with Eq. 5 (deduced from Eq. 4)

$$\Delta^i = \frac{e_s(T_a^i) - e_s(T_0)}{T_a^i - T_0} \quad (5)$$

where the saturation vapor pressure function,  $e_s(T)$ , is defined with the form (Murray 1967; Bucks 1981)

$$e_s(T) = 0.611 \exp\left(\frac{17.27(T-273)}{T-36}\right) \quad (6)$$

In Eq. 6,  $T$  is air temperature (K). Go to step 3.

3. Calculate a revised estimate of  $T_a$ ,  $T_a^{(i+1)}$ , with Eq. 7 (from Eq. 3)

$$T_a^{(i+1)} = T_0 + \frac{\gamma^* r_a Q_f}{\rho c_p (\Delta^i + \gamma^*)} - \frac{e_s(T_0) - e_0}{\Delta^i + \gamma^*} \quad (7)$$

Go to step 4.

4. If  $i = 0$ , then go to step 8. If, on the other and,  $i > 0$ , then go to step 5.

5. Calculate the incremental changes on  $T_a$  and  $\Delta$ :

(5a) Calculate the  $(i+1)th$  incremental change in  $T_a$ ,  $\delta T_a^{(i+1)}$ , with Eq. 8

$$\delta T_a^{(i+1)} = T_a^{(i+1)} - T_a^i \quad (8)$$

Go to step 5b.

(5b) Calculate the incremental change in  $\Delta$  at the  $ith$  iteration,  $\delta \Delta^i$ , with Eq. 9

$$\delta \Delta^i = \Delta^i - \Delta^{(i-1)} \quad (9)$$

Go to step 6.

6. Convergence test

(6a) If  $\delta T_a^{(i+1)} \leq 0.001K$ , then go to step 6b. If, on the other hand,  $\delta T_a^{(i+1)} > 0.001K$ , then go to step 8.

(6b) If  $\delta \Delta^i \leq 0.00001KPa/K$ , then go to step 7. If, on the other hand,  $\delta \Delta^{(i-1)} > 0.00001KPa/K$ , then go to step 8.

7. The iteration has converged and the solution is :  $T_a = T_a^i$  and  $\Delta = \Delta^i$ . Go to step 11.

8. Set  $i = i+1$  and go to step 9.

9. If  $i \leq MaxIteration$  (where  $MaxIteration$  is the maximum number of iterations allowed), then go to step 2. If, on the other hand,  $i > MaxIteration$  then go to step 10.

10. The iteration failed to converge. Go to step 12.

11. Calculate  $\ell_f$  and  $q_f$  with Eqs. 1 and 2, respectively, based on the value of  $\Delta$  obtained in step 7, and determine the corresponding evaporation flux,  $E_f$  (mm/day) with

$$E_f = 3.525 \times 10^{-2} \ell_f \quad (10)$$

Go to step 12.

12. End computation.

## 4.4.2. Simultaneous solution of equations 3 and 4 with the Newton method, model 2

### 4.4.2.a. Equations

With this approach, Eqs. 3 and 4 are solved simultaneously with the Newton method.

Accordingly, Eqs. 3 and 4 are first written in the form,  $F(\mathbf{x}) = 0$ , where  $\mathbf{x}$  is the variable vector

$$T_a - T_0 - \frac{\gamma^* r_a Q_f}{\rho c_p (\Delta + \gamma^*)} + \frac{e_s(T_0) - e_0}{\Delta + \gamma^*} = 0 \quad (11)$$

$$e_s(T_a) - e_s(T_0) - \Delta(T_a - T_0) = 0 \quad (12)$$

At each Newton iteration, say at the  $i$ th iteration, a pair of linear equations of the form given in Eq. 13 are solved simultaneously

$$\mathbf{A}(\mathbf{x}^i) \delta \mathbf{x}^{(i+1)} = -\mathbf{F}(\mathbf{x}^i) \quad (13)$$

In Eq. 13,  $\mathbf{x}^i$  is the variable vector at the  $i$ th iteration, given as

$$\mathbf{x}^i = \begin{pmatrix} T_a^i \\ \Delta^i \end{pmatrix} \quad (14)$$

$\mathbf{F}$  is the residual vector whose elements are the lefthand sides of Eqs. 11 and 12 evaluated at  $\mathbf{x} = \mathbf{x}^i$

$$\mathbf{F}(\mathbf{x}^i) = \begin{pmatrix} F_{11}(\mathbf{x})|_{\mathbf{x}=\mathbf{x}^i} \\ F_{12}(\mathbf{x})|_{\mathbf{x}=\mathbf{x}^i} \end{pmatrix} \quad (15)$$

In Eq. 15,  $F_{11}(\mathbf{x})|_{\mathbf{x}=\mathbf{x}^i}$  and  $F_{12}(\mathbf{x})|_{\mathbf{x}=\mathbf{x}^i}$  are the lefthand sides of Eqs. 11 and 12 evaluated at  $\mathbf{x} = \mathbf{x}^i$ .  $\mathbf{A}$  is a coefficient matrix given as

$$\mathbf{A}(\mathbf{x}^i) = \begin{pmatrix} [\nabla F_{11}(\mathbf{x})|_{\mathbf{x}=\mathbf{x}^i}]^T \\ [\nabla F_{12}(\mathbf{x})|_{\mathbf{x}=\mathbf{x}^i}]^T \end{pmatrix} \quad (16)$$

where  $[\nabla F_{11}(\mathbf{x})|_{\mathbf{x}=\mathbf{x}^i}]^T$  and  $[\nabla F_{12}(\mathbf{x})|_{\mathbf{x}=\mathbf{x}^i}]^T$  are the transposes of the gradient vectors of the lefthand sides of Eqs. 11 and 12, respectively, evaluated at  $\mathbf{x} = \mathbf{x}^i$  and are expressed as

$$[\nabla F_{11}(\mathbf{x})|_{\mathbf{x}=\mathbf{x}^i}]^T = \left( 1.0, -\frac{e_s(T_0) - e_0 - \frac{\gamma^* r_a Q_f}{\rho c p}}{(\Delta^i + \gamma^*)^2} \right) \quad (17)$$

$$[\nabla F_{12}(\mathbf{x})|_{\mathbf{x}=\mathbf{x}^i}]^T = \left( 4093.0 \frac{e_s(T_a^i)}{(T_a^i - 36)^2} - \Delta^i, -(T_a^i - T_0) \right) \quad (18)$$

Furthermore, in Eq. 13,  $\delta \mathbf{x}^{(i+1)}$  is the  $(i+1)$ th incremental change in the variable vector

$$\delta \mathbf{x}^{(i+1)} = \begin{pmatrix} \delta T_a^{(i+1)} \\ \delta \Delta^{(i+1)} \end{pmatrix} \quad (19)$$

### ***Computational procedure, model 2***

1. Initialize the iteration index,  $i$ , and the variables  $T_a$  and  $\Delta$ 
  - (1a) Set  $i = 0$ . Go to step 1b.
  - (1b)  $T_a^i = 1.05T_0$ . Go to step 1c.
  - (1c) Calculate  $\Delta^i$  with Eq. 5. Go to step 2.
2. Evaluate elements of the function vector,  $F_{11}$  and  $F_{12}$  [Eq. 15] at  $\mathbf{x} = \mathbf{x}^i$ , with the lefthand side expressions of Eqs. 11 and 12. Go to step 3.
3. Calculate elements of the coefficient matrix,  $\mathbf{A}^i$  [Eq. 16], at  $\mathbf{x} = \mathbf{x}^i$ , with Eqs. 17 and 18. Go to step 4.

4. Calculate the  $(i+1)$ th incremental change in the variable vector,  $\delta\mathbf{x}^{(i+1)}$ , by solving Eq. 13 with a suitable method (e.g., Creamer's rule, Watkins 2010). Go to step 5.
5. Convergence test:
  - 5a. If  $\delta T_a^{(i+1)} \leq 0.001K$ , then go to step 5b. On the other hand, if  $\delta T_a^{(i+1)} > 0.001K$ , then go to step 7.
  - 5b. If  $\delta\Delta^{(i+1)} \leq 0.00001KPa/K$ , then go to step 6. If, on the other hand,  $\delta\Delta^{(i+1)} > 0.00001KPa/K$ , then go to step 7.
6. The iteration has converged and the solution is :  $T_a = T_a^i$  and  $\Delta = \Delta^i$ . Go to step 11.
7. Update variables:
 
$$(7a) T_a^{(i+1)} = T_a^i + \delta T_a^{(i+1)} \quad (20)$$

Go to step 7b.

$$(7b) \Delta^{(i+1)} = \Delta^i + \delta\Delta^{(i+1)} \quad (21)$$

Go to step 8.
8. Set  $i = i+1$ , proceed to step 9.
9. If  $i \leq MaxIteration$ , then go to step 2. If, on the other hand,  $i > MaxIteration$  then go to step 10.
10. Iterative solution of Eqs. 3 and 4 for  $T_a$  and  $\Delta$  failed to converge. Go to step 12.
11. Calculate  $\ell_f$ ,  $E_f$ , and  $q_f$  following the description in *step 11*, under *model 1*. Go to step 12.
12. End computation.

### 4.4.3. Iterative solution of the combined equation with the Newton method, model 3

#### 4.4.3.a. Equations

With this approach, Eqs. 3 and 4 are combined into a single nonlinear equation with  $T_a$  as the variable

$$T_a - T_0 - \frac{\gamma^* r_a Q_f \zeta}{\rho c_p (\phi + \gamma^* \zeta)} + \zeta \frac{e_s(T_0) - e_0}{\phi + \gamma^* \zeta} = 0 \quad (22)$$

Equation 22 is obtained by substituting an expression for  $\Delta$

$$\Delta = \frac{\phi}{\zeta} \quad (23)$$

into Eq. 3. Thus, in Eq. 23

$$\phi = e_a(T_a) - e_s(T_0) \quad \text{and} \quad \zeta = T_a - T_0 \quad (24)$$

Noting that  $\phi$  and  $\zeta$  are both functions of  $T_a$ , it can be observed that Eq. 22 is a nonlinear equation in  $T_a$  and is solved here iteratively with the Newton method. Accordingly, in each iterative step, say at the  $i$ th iteration, the  $(i+1)$ th incremental change in  $T_a$ ,  $\delta T_a^{(i+1)}$ , is calculated with Eq. 25

$$\delta T_a^{(i+1)} = - \frac{F(T_a^i)}{\left. \frac{dF(T_a)}{dT_a} \right|_{T_a=T_a^i}} \quad (25)$$

where  $F(T_a)$  is the lefthand side of Eq. 22 evaluated at  $T_a = T_a^{(i+1)}$  and

$$\left. \frac{dF(T_a)}{dT_a} \right|_{T_a=T_a^i} = 1.0 - \left( \frac{\gamma^* r_a Q_f}{\rho c_p} - e_s(T_0) + e_0 \right) \frac{\left( \phi^i - 4093.0 \zeta^i \frac{e_s(T_a^i)}{(T_a^i - 36.0)^2} \right)}{(\phi^i + \gamma^* \zeta^i)^2} \quad (26)$$

### ***Computational procedure, model 3***

1. Initialize the iteration index,  $i$ , and variable,  $T_a$ .
  - (1a) Set the iteration index,  $i$ , to 0. Go to step 1b.
  - (1b) Set  $T_a^i = 1.05T_0$ . Go to step 2.
2. Calculate  $F(T_a^i)$  with the righthand side expression of Eq. 22. Go to step 3.
3. Calculate  $(dF(T_a)/dT_a)_{T_a=T_a^i}$  with Eq. 26. Go to step 4.
4. Calculate the  $(i+1)$ th incremental change in the variable vector,  $\delta T_a^{(i+1)}$ , with Eq. 25. Go to step 5.
5. Convergence test: If  $\delta T_a^{(i+1)} \leq 0.001K$ , then go to step 6. On the other hand, if  $\delta T_a^{(i+1)} > 0.001K$ , then go to step 7.
6. The iteration has converged and the solution is  $T_a = T_a^i$ . Go to step 11.
7. Update variable: set  $T_a^{(i+1)} = T_a^i + \delta T_a^{(i+1)}$ . Go to step 8.
8. Set  $i = i+1$ , proceed to step 9.
9. If  $i \leq \text{MaxIteration}$ , then go to step 2. If, on the other hand,  $i > \text{MaxIteration}$  then go to step 10.
10. Iterative solution of Eq. 22 failed to converge. Go to step 12.
11. Calculate  $\Delta$  with Eq. 5 as a function  $T_a$  computed in step 6 above and calculate  $\ell_f$ ,  $E_f$ , and  $q_f$  following step 11 described under *model 1*. Go to step 12.
12. End computation.

#### 4.4.4. Simultaneous iterative solution of the modified forms of Eqs. 1 to 3 with the Newton method, model 4

##### 4.4.4.a. Equations

With this approach, a system consisting of modified forms of Eqs. 1 to 3 are solved simultaneously with the Newton method. The modified equations given in the form of  $F(\mathbf{x}) = 0$  are

$$\ell_f - \frac{\phi Q_f}{\phi + \gamma^* \zeta} - \rho c_p \zeta \frac{e_s(T_0) - e_0}{(\phi + \gamma^* \zeta) r_a} = 0 \quad (27)$$

$$q_f - \frac{\zeta \gamma^* Q_f}{\phi + \gamma^* \zeta} + \rho c_p \zeta \frac{e_s(T_0) - e_0}{(\phi + \gamma^* \zeta) r_a} = 0 \quad (28)$$

$$T_a - T_0 - \frac{\zeta \gamma^* r_a Q_f}{\rho c_p (\phi + \gamma^* \zeta)} + \zeta \frac{e_s(T_0) - e_0}{\phi + \gamma^* \zeta} = 0 \quad (29)$$

Note that Eqs. 27 to 29 are obtained by substituting an expression for  $\Delta$  (Eq. 23) into Eqs. 1 to 3.

Considering that  $\phi$  and  $\zeta$  (Eq. 24) are functions of  $T_a$ , it can be observed that Eqs. 27 to 29 constitute a nonlinear system of equations in the variables  $\ell_f$ ,  $q_f$ , and  $T_a$ . Accordingly, in each Newton iteration, say in the  $(i+1)$ th iteration, a system of linear equations of the form given in Eq. 13 is solved simultaneously. However, compared to model 2, which involves a pair of equations with two variables, the system applicable to model 4 consists of three equations with three variables. Thus, the corresponding residuals,  $F(\mathbf{x}^i)$ , and variable,  $\mathbf{x}^i$ , vectors are given as

$$F(\mathbf{x}^i) = \begin{pmatrix} F_{27}(\mathbf{x})|_{x=x^i} \\ F_{28}(\mathbf{x})|_{x=x^i} \\ F_{29}(\mathbf{x})|_{x=x^i} \end{pmatrix} \quad \text{and} \quad \mathbf{x}^i = \begin{pmatrix} \ell_f^i \\ q_f^i \\ T_a^i \end{pmatrix} \quad (30)$$

where  $F_{27}(\mathbf{x})|_{\mathbf{x}=\mathbf{x}^i}$ ,  $F_{28}(\mathbf{x})|_{\mathbf{x}=\mathbf{x}^i}$ , and  $F_{29}(\mathbf{x})|_{\mathbf{x}=\mathbf{x}^i}$  are the expressions on the lefthand sides of Eqs. 27, 28, and 29, respectively, evaluated at  $\mathbf{x} = \mathbf{x}^i$ .  $\ell_f^i$ ,  $q_f^i$ , and  $T_a^i$  are the latent heat, sensible heat, and final air temperature values at the  $i$ th iteration, respectively.

The coefficient matrix,  $\mathbf{A}$ , is given as

$$\mathbf{A}(\mathbf{x}^i) = \begin{pmatrix} [\nabla F_{27}(\mathbf{x})|_{\mathbf{x}=\mathbf{x}^i}]^T \\ [\nabla F_{28}(\mathbf{x})|_{\mathbf{x}=\mathbf{x}^i}]^T \\ [\nabla F_{29}(\mathbf{x})|_{\mathbf{x}=\mathbf{x}^i}]^T \end{pmatrix} \quad (31)$$

where  $[\nabla F_{27}(\mathbf{x})|_{\mathbf{x}=\mathbf{x}^i}]^T$ ,  $[\nabla F_{28}(\mathbf{x})|_{\mathbf{x}=\mathbf{x}^i}]^T$ , and  $[\nabla F_{29}(\mathbf{x})|_{\mathbf{x}=\mathbf{x}^i}]^T$  are the transposes of the gradient vectors of Eqs. 27, 28, and 29, respectively, evaluated at  $\mathbf{x} = \mathbf{x}^i$ , and are expressed as

$$[\nabla F_{27}(\mathbf{x})|_{\mathbf{x}=\mathbf{x}^i}]^T = \begin{pmatrix} \left( 4093.0 \zeta^i \frac{e_s(T_a^i)}{(T_a^i - 36.0)^2} \right) \left( \frac{\rho c_p}{r_a} (e_s(T_0) - e_0) - \gamma^* Q_f \right) \\ 1.0, 0.0, \frac{+\phi \left( \gamma^* Q_f - \frac{\rho c_p}{r_a} (e_s(T_0) - e_0) \right)}{(\phi^i + \gamma^* \zeta^i)^2} \end{pmatrix} \quad (32)$$

$$[\nabla F_{28}(\mathbf{x})|_{\mathbf{x}=\mathbf{x}^i}]^T = \begin{pmatrix} \left( \phi^i - 4093.0 \zeta^i \frac{e_s(T_a^i)}{(T_a^i - 36.0)^2} \right) \\ 0.0, 1.0, \left( \frac{\rho c_p}{r_a} (e_s(T_0) - e_0) - \gamma^* Q_f \right) \frac{\left( \phi^i - 4093.0 \zeta^i \frac{e_s(T_a^i)}{(T_a^i - 36.0)^2} \right)}{(\phi^i + \gamma^* \zeta^i)^2} \end{pmatrix} \quad (33)$$

$$[\nabla F_{29}(\mathbf{x})|_{\mathbf{x}=\mathbf{x}^i}]^T = \begin{pmatrix} \left( \phi^i - 4093.0 \zeta^i \frac{e_s(T_a^i)}{(T_a^i - 36.0)^2} \right) \\ 0.0, 0.0, 1.0 + \left( e_s(T_0) - e_0 - \frac{\gamma^* r_a Q_f}{\rho c_p} \right) \frac{\left( \phi^i - 4093.0 \zeta^i \frac{e_s(T_a^i)}{(T_a^i - 36.0)^2} \right)}{(\phi^i + \gamma^* \zeta^i)^2} \end{pmatrix} \quad (34)$$

Furthermore,  $\delta \mathbf{x}^{(i+1)}$  is the  $(i+1)$ th incremental change in the variable vector, given as

$$\delta \mathbf{x}^{(i+1)} = \begin{pmatrix} \delta \ell_f^{(i+1)} \\ \delta q_f^{(i+1)} \\ \delta T_a^{(i+1)} \end{pmatrix} \quad (35)$$

where  $\delta \ell_f^{(i+1)}$ ,  $\delta q_f^{(i+1)}$ , and  $\delta T_a^{(i+1)}$  are the  $(i+1)$ th incremental change in the latent heat, sensible heat, and final air temperature, respectively, defined in accordance with the form given in Eq. 8.

#### 4.4.4.b. Iterative algorithm for computing $T_a$ , $\ell_f$ , and $q_f$ , model 4

1. Initialize the iteration index,  $i$ , and variables
  - (1a) Set  $i = 0$ . Go to step 1b.
  - (1b) Set  $T_a^i = 1.05T_0$ . Go to step 1c.
  - (1c) Set  $\ell_f^i = \ell_f(T_a^i)$ , Eq. 27. Go to step 1d.
  - (1d) Set  $q_f^i = q_f(T_a^i)$ , Eq. 28. Go to step 2.
2. Evaluate elements of the function vector, Eq. 30, at  $\mathbf{x} = \mathbf{x}^i$  with Eqs. 27-29. Go to step 3.
3. Calculate elements of the coefficient matrix,  $\mathbf{A}^i$  [Eq. 31], at  $\mathbf{x} = \mathbf{x}^i$ , with Eqs. 32 to 34. Go to step 4.
4. Calculate the  $(i+1)$ th incremental change in the variable vector,  $\delta \mathbf{x}^{(i+1)}$ , by solving a form of Eq. 13 applicable to model 4 with a suitable method (e.g., Watkins 2010). Go to step 5.
5. Convergence test:
  - (5a) If  $\delta \ell_f^{(i+1)} \leq 0.001 W/m^2$ , then go to step 5b. If, on the other hand,  $\delta \ell_f^{(i+1)} > 0.001 W/m^2$ , then go to step 8.
  - (5b) If  $\delta q_f^{(i+1)} \leq 0.001 W/m^2$ , then go to step 5c. If, on the other hand,  $\delta q_f^{(i+1)} > 0.001 W/m^2$ , then go to step 8.

(5a) If  $\delta T_a^{(i+1)} \leq 0.001K$ , then go to step 6. On the other hand, if  $\delta T_a^{(i+1)} > 0.001K$ , then go to step 8.

6. The iteration has converged and the solution is:  $T_a = T_a^i$ ,  $\ell_f = \ell_f^i$ , and  $q_f = q_f^i$ . Go to step 7.

7. Calculate:

(7a)  $\Delta$  with Eq. 5 based on the  $T_a$  value given in step 6. Go to step 7b.

(7b)  $E_f$  with Eq. 10. Go to step 12.

8. Update variables

$$T_a^{(i+1)} = T_a^i + \delta T_a^{(i+1)} \quad (36)$$

$$\ell_f^{(i+1)} = \ell_f^i + \delta \ell_f^{(i+1)} \quad (37)$$

$$q_f^{(i+1)} = q_f^i + \delta q_f^{(i+1)} \quad (38)$$

Go to step 9.

9. Set  $i = i+1$ , proceed to step 10.

10. If  $i \leq \text{MaxIteration}$ , then go to step 2. If, on the other hand,  $i > \text{MaxIteration}$  then go to step 11.

11. Iterative solution of Eqs. 27 to 29 failed to converge. Go to step 12.

12. End computation.

#### 4.5. Model evaluation

Evaluation of the alternative numerical solutions was focused on assessing the soundness of the mathematical formulation and programmatic implementation of the numerical algorithms of the alternative models (models 1, 2, 3, and 4). It was conducted based on comparison of the variable

estimates computed with these models to those reported by McArthur (1990), considered here a benchmark solution.

#### **4.5.1. Data description**

Three data sets obtained from the study presented by McArthur (1990) were used in model evaluation. These data are summarized in Table 1 under the labels of data set 1, 2, and 3. Each data set of McArthur considers a wet surface with a canopy resistance of 0s/m, resistance to heat transfer,  $r_h$ , of 100s/m, and a relatively strong sunshine with net external heat flux into the air of 500 W/m<sup>2</sup>. The vapor pressure deficit was set to zero for each data set and the measured air temperatures were 273K for data set 1, 293K for data set 2, and 313K for data set 3. In the current study, the resistance to heat transfer,  $r_h$ , was set equal to the aerodynamic resistance,  $r_a$ , and the canopy resistance parameter was set equal to the bulk surface resistance parameter,  $r_s$ , of the FAO Penman–Monteith equation (Allen et al. 1998).

#### **4.5.2. Summary of results reported by McArthur (1990)**

The results reported by McArthur (1990) show that the differences in the estimates of  $\ell_f$  obtained with the iterative approach and those calculated with the conventional model vary between about 1.5% (data set 3) and 40.0% (data set 1) of the values obtained with the conventional approach. Although not reported by McArthur, it can be shown that the residuals between estimates of  $T_a$  presented by McArthur and those of the conventional model range from 0.3% (data set 3) to 1.9% (data set 1) of those calculated with the conventional model. The corresponding differences

**Table 1.** Weather, crop, and related evaporation parameters

Variable/parameter name	Unit	McArthur's data sets			Additional data sets			
		Data set 1	Data set 2	Data set 3	Data set 4	Data set 5	Data set 6	Data Set 7
Measured air temperature, $T_0$	K	273	293	313	278	303	308	293
Psychrometer constant, $\gamma$	KPa/K		0.066		0.066	0.066	0.066	0.066
External heat flux, $Q_f$	W/m <sup>2</sup>		500		300	420	650	400
Air density, $\rho$	Kg/m <sup>3</sup>		1.204		1.204	1.204	1.204	1.204
Heat capacity of air at constant pressure, $c_p$	J/Kg		1005		1005	1005	1005	1005
Vapor pressure, $e_0^{(*)}$	KPa	0.611	2.343	7.398	0.5	3.504	5.2	0.243
Wind velocity measurement height, $z_m^{(**)}$	m		-		2	2	2.5	2
Wind speed at measurement, $u(z)^{(**)}$	m/s		-		1	1.2	3.5	3
Vapor pressure measurement height, $z_h^{(**)}$	m		-		2	2	2.5	2
Roughness length, momentum transfer, $z_{om}^{(**)}$	m		-		0.0738	0.0148	0.0431	0.0923
Roughness length, heat and vapor transfer, $z_{oh}^{(**)}$	m		-		0.0074	0.0015	0.0043	0.0092
Zero plane displacement height, $d^{(**)}$	m		-		0.400	0.080	0.233	0.500
Crop height, $h^{(**)}$	m		-		0.6	0.12	0.35	0.75
Bulk surface resistance, $r_s$	s/m		0		40	100	120	60
Aerodynamic resistance, $r_a^{(***)}$	s/m		100		-	-	-	-

(\*) For McArthur's data sets (i.e., data sets 1 to 3), the vapor pressures correspond to saturated conditions for the respective temperatures.

(\*\*) For McArthur's data sets, the resistance to heat transfer (which is the same as aerodynamic resistance) is set to 100s/m. Thus, the weather, crop, and other parameters required for the determination of the aerodynamic resistance are not specified.

(\*\*\*) For the additional data sets (data sets 4 to 7) the aerodynamic resistance is not specified at the input, because it is calculated as a function of the weather, crop, and other parameters specified at the input

between estimates of  $\Delta$  obtained with the two methods vary between 12.0% (data set 3) and 79.3% (data set 1) of those computed with the conventional approach. McArthur's solution (obtained with the sequential function-evaluation scheme) will now be compared to the solutions produced by the alternative models, developed in the current study.

#### **4.5.3. Comparison of variable estimates obtained with the alternative models and McArthur's model**

The computational procedures newly proposed here (i.e., model 2, 3, and 4) and the programmatic implementation of McArthur's approach (referred here as model 1) are evaluated by comparing estimates of  $\ell_f$ ,  $q_f$ ,  $E_f$ ,  $T_a$ , and  $\Delta$  computed with each of the models with those reported by McArthur (1990). The variable estimates obtained with each model and those reported by McArthur are shown in Tables 2a and 2b. In addition, a summary of the percent absolute residuals between the estimates obtained with each of the alternative models and those reported by McArthur are presented in Tables 2a and 2b. Although McArthur did not provide data on  $q_f$  and  $E_f$ ,  $q_f$  and  $E_f$  values are included in Tables 2a and 2b for completeness and were calculated with Eqs. 2 and 10 based on the  $\Delta$  and  $\ell_f$  values reported by McArthur (1990).

The data reported by McArthur shows that  $\ell_f$  varies between a minimum of 274.0 (data set 1) and a maximum of 435.0 W/m<sup>2</sup> (data set 3), Table 2a. The final air temperature (which is referred to as surface temperature by McArthur) ranges between 290.6 and 318.0K, while estimates of  $\Delta$  vary from 0.0796 (data set 1) to 0.442KPa/K (data set 3). Furthermore, a cursory look at Tables 2a and 2b show that for each data set the variable estimates obtained with the four models are practically identical. Thus, subsequent discussion on the variable estimates will make no distinction between outputs of alternative models.

**Table 2a.** Comparison of variable estimates computed with each of models 1 and 2 with those presented by McArthur (1990), McArthur’s data sets

Variable name	Unit	Model outputs								
		McArthur’s model			Model 1			Model 2		
		Data set 1	Data set 2	Data set 3	Data set 1	Data set 2	Data set 3	Data set 1	Data set 2	Data set 3
Latent heat flux, $\ell_f$	W/m <sup>2</sup>	274.0	372.0	435.0	277.1	373.0	435.6	277.1	373.0	435.6
Sensible heat flux, $q_f^{(*)}$	W/m <sup>2</sup>	226.6	128.4	65.0	222.9	127.0	64.4	222.9	127.0	64.4
Evaporation flux, $E_f^{(*)}$	mm/day	9.7	13.1	15.3	9.8	13.1	15.4	9.8	13.1	15.4
Final air temperature, $T_a$	K	290.6	303.0	318.0	291.4	303.5	318.3	291.4	303.5	318.3
Saturation vapor pressure related slope parameter, $\Delta$	KPa/K	0.0796	0.191	0.442	0.0821	0.1938	0.4465	0.0821	0.1938	0.4465

Percent absolute residuals<sup>(\*\*\*)</sup>

Variable name	Unit	-	between McArthur’s model and model 1			between McArthur’s model and model 2		
			Min	Max	Av	Min	Max	Av
Latent heat flux, $\ell_f$	% <sup>(**)</sup>	-	0.140	1.146	0.515	0.140	1.146	0.515
Sensible heat flux, $q_f^{(*)}$	%	-	0.876	1.672	1.204	0.876	1.671	1.204
Evaporation flux, $E_f^{(*)}$	%	-	0.140	1.146	0.515	0.140	1.151	0.517
Final air temperature, $T_a$	%	-	0.101	0.281	0.182	0.101	0.281	0.182
Saturation vapor pressure related slope parameter, $\Delta$	%	-	1.016	3.110	1.858	1.016	3.109	1.858

<sup>(\*)</sup> McArthur (1990) did not provide estimates of sensible heat and evaporation fluxes. The values presented here were calculated, for completeness, with Eq. 2 and 10 based on the  $\Delta$  values presented by McArthur.

<sup>(\*\*)</sup> For each variable and data set combination, percent residuals were calculated with:

$$\text{absolute residual} = \frac{|\text{variable estimate with model 1 or 2} - \text{variable estimate by McArthur}|}{\text{variable estimate by McArthur}} \cdot 100$$

<sup>(\*\*\*)</sup> Min, Max, and Av are the minimum, maximum, and average percent absolute residuals, respectively

**Table 2b.** Comparison of variable estimates computed with each of model 3 and 4 with those presented by McArthur (1990), McArthur’s data sets

Variable name	Unit	Model outputs								
		McArthur’s models			Model 3			Model 4		
		Data set 1	Data set 2	Data set 3	Data set 1	Data set 2	Data set 3	Data set 1	Data set 2	Data set 3
Latent heat flux, $\ell_f$	W/m <sup>2</sup>	274.0	372.0	435.0	277.1	373.0	435.6	277.2	372.9	435.6
Sensible heat flux, $q_f^{(*)}$	W/m <sup>2</sup>	226.6	128.4	65.0	222.9	127.0	64.4	222.8	127.1	64.4
Evaporation flux, $E_f^{(*)}$	mm/day	9.7	13.1	15.3	9.8	13.2	15.4	9.8	13.1	15.4
Final air temperature, $T_a$	K	290.6	303.0	318.0	291.4	303.5	318.3	291.4	303.5	318.3
Saturation vapor pressure related slope parameter, $\Delta$	KPa/K	0.0796	0.191	0.442	0.0821	0.1938	0.4465	0.0821	0.1938	0.4465

Percent absolute residuals (\*\*\*)

Variable name	Unit	-	between McArthur’s model and model 3			between McArthur’s model and model 4		
			Min	Max	Av	Min	Max	Av
Latent heat flux, $\ell_f$	% (**)	-	0.140	1.146	0.515	0.134	1.177	0.519
Sensible heat flux, $q_f^{(*)}$	%	-	0.876	1.671	1.204	0.842	1.705	1.193
Evaporation flux, $E_f^{(*)}$	%	-	0.140	1.146	0.515	0.134	1.177	0.519
Final air temperature, $T_a$	%	-	0.101	0.281	0.182	0.102	0.279	0.182
Saturation vapor pressure related slope parameter, $\Delta$	%	-	1.016	3.109	1.858	1.020	3.087	1.855

(\*) McArthur (1990) did not provide estimates of sensible heat and evaporation fluxes. The values presented here were calculated, for completeness, with Eq. 2 and 10 based on the  $\Delta$  values presented by McArthur.

(\*\*) For each variable and data set combination, percent residuals were calculated with

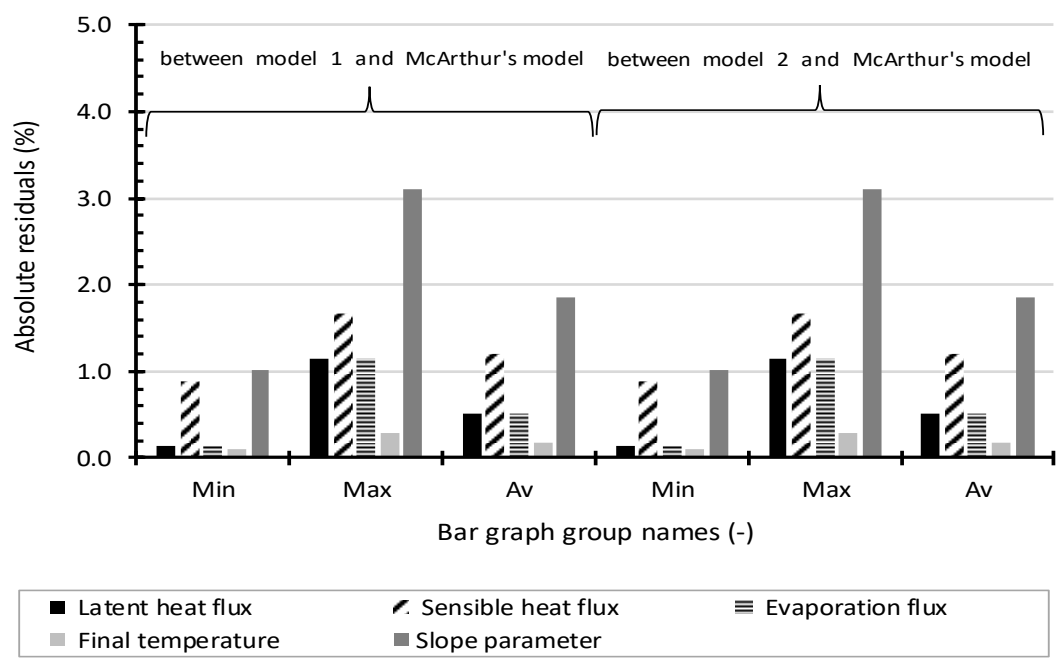
$$\text{absolute residual} = \frac{|\text{variable estimate with model 1 or 2} - \text{variable estimate by McArthur}|}{\text{variable estimate by McArthur}} 100$$

(\*\*\*) Min, Max, and Av are the minimum, maximum, and average percent absolute residuals, respectively

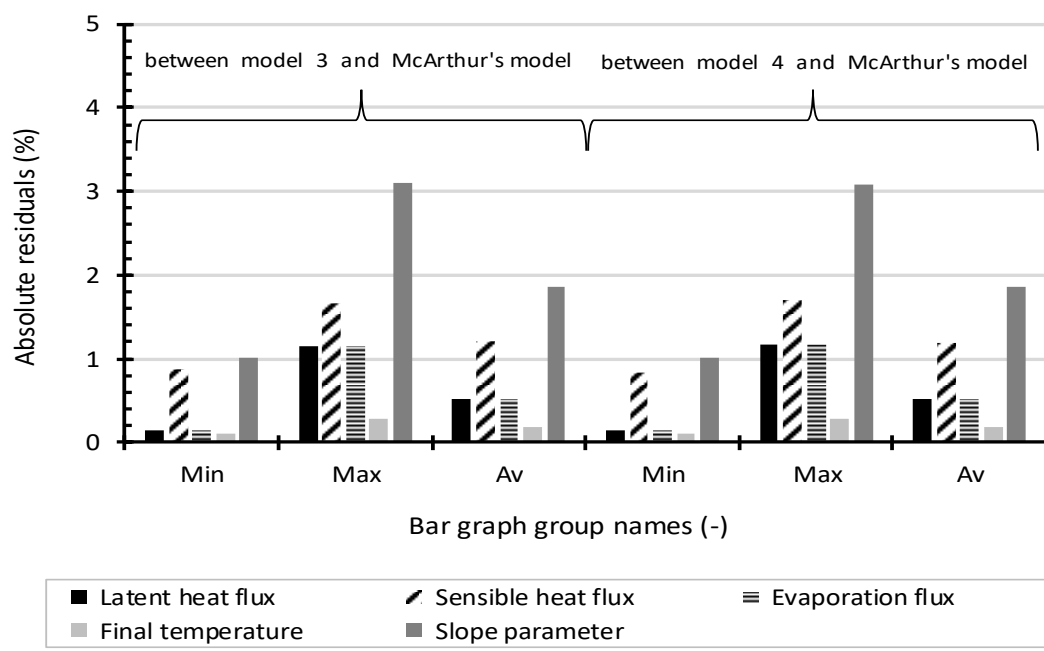
Accordingly, it can be observed from Tables 2a and 2b that estimates of  $\ell_f$  obtained with the models, overall, vary between a minimum of about  $277.1\text{W/m}^2$  (data set 1) and a maximum of  $435.6\text{W/m}^2$  (data set 3) and those of  $E_f$  ranges from 9.8 to 15.4mm. On the other hand, estimates of  $T_a$  vary between a minimum of  $291.4\text{W/m}^2$  (data set 1) and a maximum of  $318.3\text{W/m}^2$  (data set 3) and  $\Delta$  ranges from 0.0821 (data set 1) to 0.4465KPa/K (data set 3). By comparison, sensible heat,  $q_f$ , vary between a minimum of  $64.4\text{W/m}^2$  (data set 3) and a maximum of  $222.9\text{W/m}^2$  (data set 1).

A summary of the absolute residuals between variable estimates obtained with each of the models and those reported by McArthur are given in Tables 2a and 2b. However, in order to allow for a more direct visual comparison, the residuals are also plotted in grouped bar charts, Figure 1a for models 1 and 2 and Figure 1b for models 3 and 4. A closer look at Figures 1a and 1b (and Tables 2a and 2b) shows that the maximum absolute residual between the variable estimates obtained with the alternative models and those of McArthur occur for  $\Delta$  and it is about 3.1% and the average is 1.9%. The variable with the second largest residuals is the sensible heat flux, with a maximum of about 1.7%, the average value being 1.2%. On the other hand, the smallest residuals between the parameter estimates obtained with the proposed models and those of McArthur was obtained for the final air temperature, the maximum being about 0.3% and the average 0.2%. The latent heat and evaporation fluxes fall somewhere in between with a maximum absolute residual of about 1.2% and an average value of 0.5%.

Overall, the percent absolute residuals summarized in Figures 1a and 1b and Tables 2a and 2b suggest that the variable estimates obtained with the proposed models and those reported by McArthur are generally close. Estimates for  $T_a$ , and the more important variables of latent heat flux and evaporation flux, are all on the average within about 0.5% of those reported by



(a)



(b)

Figure 1. Absolute residuals between variable estimates obtained with (a) Models 1 and 2 and McArthur's model and (b) Models 3 and 4 and McArthur's model (McArthur's data set)

McArthur. However, the average residuals for  $\Delta$  and  $q_f$  are greater than 1.0% (the maximum being 3.1%), hence slightly larger than what could be considered sufficiently small when comparing outputs of numerical solutions. Perhaps, differences in the programmatic implementation of the models (particularly model 1) in the current study and the specifics of (what appears to be a manual) calculation procedure used by McArthur (1990) may account for the slightly larger differences than would be desirable. Given that models 1, 2, 3, and 4 produce essentially identical outputs (Table 2), all the models were considered for further analysis.

#### **4.6. Model selection**

Results of intercomparison of models (conducted based on all the data sets given in Table 1) combined with considerations of such criteria as numerical efficiency, robustness, and simplicity were used in the selection of a model for further analysis, among the four alternatives.

##### **4.6.1. Data description**

Four more hypothetical data sets (labeled as additional data sets in Table 1), covering a wider range of natural evaporation scenarios are used in model selection. For these data sets, the vapor pressure deficits range between 0.373 to 2.1 kPa, which represent relatively humid and rather dry air conditions, respectively. The measured air temperature ranges from 278 to 308 K and the external heat flux varies between 300 and 650 W/m<sup>2</sup>. Note that for the additional data sets, the aerodynamic resistance values are not specified in Table 1, because they are not inputs to the model. Instead, they were computed as a function of wind speed and roughness lengths and zero plane displacement, both calculated as a function of crop height (Table 1) following the approach described by Allen et al. (1998). Hence, they are summarized in an output data table.

#### **4.6.2. Comparison of the outputs of the alternative models based on additional data**

Evaporation variable estimates computed with each of the alternative models and the corresponding percent absolute residuals for all data sets are presented in Tables 3a and 3b, respectively. Note that, for convenience, the model outputs section of Table 3a simply replicates the data presented in Tables 2a and 2b (i.e., variable estimates obtained with models 1, 2, 3, and 4 for the McArthur data sets) in a different format. The percent absolute residuals section of Table 3a, on the other hand, presents new data. More discussion on the data will be presented shortly. Before that, a summary of the absolute residuals between the variable estimates obtained with model 1, 2, 3, and 4 (Tables 3a and 3b) will be highlighted.

A close look at the absolute residuals section of Tables 3a and 3b suggests that the variable estimates obtained with the models are essentially identical. However, in order to allow for a more direct visual comparison, a summary of the residuals covering all the data sets are presented in a group bar chart (Figure 2). As can be noted from Figure 2 (and also from Tables 3a and 3b), the percent absolute residuals between the variable estimates obtained with model 2 and those of mode 1 and between model 3 and those of model 1 are within 0.005% of those computed with model 1. The maximum percent absolute residual between variable estimates obtained with model 4 and 1 is 0.09% of those computed with model 1 and it is associated with estimates of sensible heat flux. Furthermore, Figure 2 shows that the residuals for all the other variables and across all the data sets are less than 0.06%.

The fact that the variable estimates obtained with the proposed models are essentially identical, across all the data sets, suggests that these algorithms can be considered equally acceptable.

**Table 3a.** Comparison of variable estimates computed with each of models 2, 3, and 4 with those obtained using model 1, McArthur’s data sets

Variable name	Unit	Model outputs											
		Model 1			Model 2			Model 3			Model 4		
		Data set 1	Data set 2	Data set 3	Data set 1	Data set 2	Data set 3	Data set 1	Data set 2	Data set 3	Data set 1	Data set 2	Data set 3
Latent heat flux, $\ell_f$	W/m <sup>2</sup>	277.1	373.0	435.6	277.1	373.0	435.6	277.1	373.0	435.6	277.2	372.9	735.6
Sensible heat, $q_f$	W/m <sup>2</sup>	222.9	127.0	64.4	222.9	127.0	64.4	222.9	127.0	64.4	222.8	127.1	64.4
Evaporation flux, $E_f^{(*)}$	mm/day	9.8	13.1	15.4	9.8	13.1	15.4	9.8	13.1	15.4	9.8	13.1	15.4
Final air temperature, $T_a$	K	291.4	303.5	318.3	291.4	303.5	318.3	291.4	303.5	318.3	291.4	303.5	318.3
Saturation vapor pressure related slope parameter, $\Delta$	KPa/K	0.0821	0.1938	0.4465	0.0821	0.1938	0.4465	0.0821	0.1938	0.4465	0.0821	0.1938	0.4465

Variable name	Unit	-	Percent absolute residuals between estimates obtained with model 1 and those calculated with model 2, 3, and 4 (**)								
			Models 1 and 2			Models 1 and 3			Models 1 and 4		
			Min	Max	Av	Min	Max	Av	Min	Max	Av
Latent heat flux, $\ell_f$	(%) <sup>(*)</sup>		0.0000	0.0005	0.0002	0.0000	0.0005	0.0002	0.006	0.030	0.016
Sensible heat flux, $q_f^{(*)}$	(%)	-	0.0001	0.0006	0.0004	0.0000	0.0006	0.0003	0.033	0.034	0.033
Evaporation flux, $E_f^{(*)}$	(%)	-	0.0000	0.0046	0.0016	0.0000	0.0005	0.0002	0.006	0.030	0.016
Final air temperature, $T_a$	(%)	-	0.0000	0.0001	0.0001	0.0000	0.0000	0.0000	0.001	0.002	0.001
Saturation vapor pressure related slope parameter, $\Delta$	(%)	-	0.0001	0.0011	0.0006	0.0000	0.0011	0.0005	0.004	0.022	0.012

(\*) For each variable and data set combination percent absolute residuals were calculated with

$$\text{absolute residual} = \frac{|\text{variable estimate with model 2, 3, or 4} - \text{variable estimate with model 1}|}{\text{variable estimate with model 1}} 100$$

(\*\*) Min, Max, Av are the minimum, maximum, and average percent absolute residuals, respectively.

**Table 3b.** Comparison of variable estimates computed with each of models 2, 3, and 4 with those obtained using model 1, additional data sets

Variable name	Unit	Model outputs															
		Model 1				Model 2				Model 3				Model 4			
		Data set 4	Data set 5	Data set 6	Data set 7	Data set 4	Data set 5	Data set 6	Data set 7	Data set 4	Data set 5	Data set 6	Data set 7	Data set 4	Data set 5	Data set 6	Data set 7
Latent heat flux, $\ell_f$	W/m <sup>2</sup>	191.3	339.8	520.5	683.3	191.3	339.8	520.5	683.3	191.3	339.8	520.5	683.3	191.2	339.8	520.5	683.2
Sensible heat flux, $q_f^{(*)}$	W/m <sup>2</sup>	108.7	80.2	129.5	-283.3	108.7	80.2	129.5	-283.3	108.7	80.2	129.5	-283.3	108.8	80.2	129.5	-283.2
Evaporation flux, $E_f^{(*)}$	mm/day	6.7	12.0	18.3	24.1	6.7	12.0	18.3	24.1	6.7	12.0	18.3	24.1	6.7	12.0	18.3	24.1
Final air temperature, $T_a$	K	286.8	314.5	312.5	286.4	286.8	314.5	312.5	286.4	286.8	314.5	312.5	286.4	286.9	314.5	312.5	286.4
Saturation vapor pressure related slope parameter, $\Delta$	KPa/K	0.0805	0.3265	0.3478	0.1217	0.0805	0.3265	0.3478	0.1217	0.0805	0.3265	0.3478	0.1217	0.0805	0.3265	0.3478	0.1217

		-	Percent absolute residuals between estimates obtained with model 1 and those calculated with model 2, 3, and 4 (**)								
			Models 1 and 2			Models 1 and 3			Models 1 and 4		
			Min	Max	Av	Min	Max	Av	Min	Max	Av
Latent heat flux, $\ell_f$	(%) <sup>(*)</sup>	-	0.0000	0.0002	0.0001	0.0000	0.0004	0.0002	0.0059	0.0541	0.0206
Sensible heat flux, $q_f^{(*)}$	(%)	-	0.0000	0.0004	0.0002	0.0001	0.0007	0.0003	0.0218	0.0915	0.0437
Evaporation flux, $E_f^{(*)}$	(%)	-	0.0000	0.0002	0.0001	0.0000	0.0004	0.0002	0.0059	0.0541	0.0206
Final air temperature, $T_a$	(%)	-	0.0000	0.0002	0.0001	0.0000	0.0000	0.0000	0.0003	0.0028	0.0012
Saturation vapor pressure related slope parameter, $\Delta$	(%)	-	0.0000	0.0007	0.0003	0.0001	0.0012	0.0006	0.0025	0.0271	0.0107

(\*) For each variable and data set combination percent absolute residuals were calculated with:

$$\text{absolute residual} = \frac{|\text{variable estimate with model 2, 3, or 4} - \text{variable estimate with model 1}|}{\text{variable estimate with model 1}} 100$$

(\*\*) Min, Max, Av are the minimum, maximum, and average percent absolute residuals, respectively.

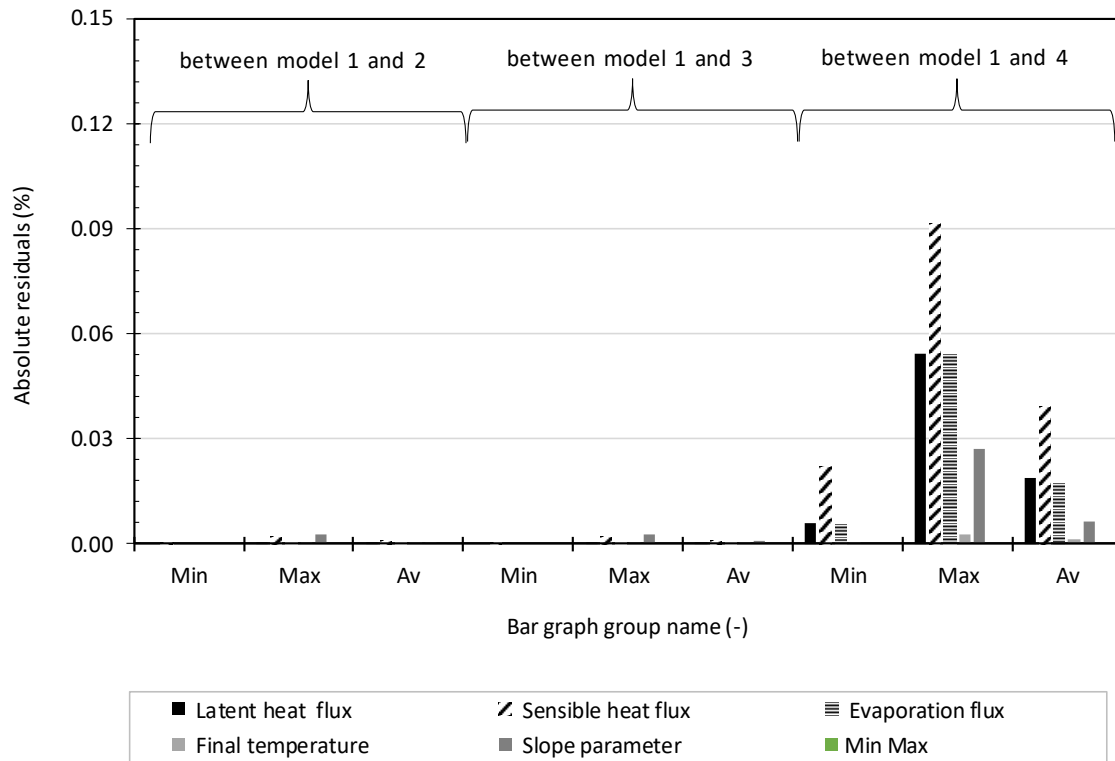


Figure 2. Absolute residuals between variable estimates computed with each of models 2, 3, and 4 and those obtained with model 1 (all data sets, Table 1)

#### 4.6.3. Numerical robustness, efficiency, and simplicity

The results show that each of the numerical algorithms, presented here, were able to solve all the evaporation problems (i.e., data sets) considered. This implies that all the models presented here (i.e., model 1, 2, 3, and 4) are equally robust, although with varying degrees of efficiency. A close look at the iteration data shows that model 1 required 5 to 9 iterations to converge to the solutions for all the problems considered here, while model 2 converged to the solution within 2 to 4 iterations. Model 3, on the other hand, obtained the solution to all the seven data sets in 2 iterations. By contrast, model 4 required by far the largest number of iterations, ranging between

169 and 1033 to obtain the solutions. While these differences in apparent numerical efficiency may be significant in terms of CPU time, since the problem concerns the solution of small system of equations (at most three equations in three variables), the actual runtimes for each of these models are nearly indistinguishable and are about a few seconds in a regular PC.

The preceding observations suggest that from the perspectives of accuracy and numerical robustness and efficiency (in the sense of required model runtime), each of the models represent a comparable alternative to any of the other alternatives for estimating natural evaporation from a cropped field. However, the fact that model 1 is based on function evaluation implies that its implementation does not require any specialized numerical method. By comparison, models 2, 3, and 4 use Newton iteration method to solve a minimum of 1 and a maximum of 3 nonlinear equations with 1 to 3 variables, respectively. The implication is that model 1 is simpler than the other models, both conceptually and in terms of its numerical formulation and programmatic implementation, which is an advantage. Thus, model 1 was considered for further analysis, which involves comparison of model 1 with the conventional model. Before that, however, a discussion on the structure of the Penman-Monteith equations and its effect on numerical solutions will be presented.

#### **4.6.4. An observation on the structure of the equations and its effect on numerical solutions**

Equations 1 to 4 are a coupled system of equations and hence in principle the complete set needs to be solved simultaneously. However, results presented earlier show that solutions produced by models 1, 2, and 3 (representing simpler formulation of the evaporation problem) are as accurate as the solutions obtained with simultaneous iterative solution of the complete set, model 4. A close look at the structure of Eqs. 1 to 4 reveals a potential explanation for this apparent

incompatibility between observations made on numerical outputs computed with models 1, 2, 3, and 4, on one hand, and basic mathematical requirements, on the other.

A look at Eqs. 1 and 2 shows that these equations have one variable each ( $\ell_f$  in the case of Eq. 1 and  $q_f$  in the case of Eq. 2) that do not appear in any of the other equations. Furthermore, Eqs. 1 and 2 share only the variable  $\Delta$  with the other equations and among themselves as well. This observation suggests that in their current form, Eqs. 1 and 2 are not as strongly coupled to Eqs 3 and 4 and with each other as well, as for instance Eq. 3 is to that of Eq. 4 or vice-versa (where both equations are functions of  $T_a$  and  $\Delta$ ). As noted earlier, this observation points to the possibility that a simpler formulation, than the iterative solution of the complete set, in which Eqs. 3 and 4 are decoupled from Eqs. 1 and 2 may yield sufficiently accurate, but more efficient and robust, solutions.

In fact, a close examination of the algorithm of the simpler models (models 1, 2, and 3) provides evidence that directly support this inference. A look at Eqs. 1 to 4 reveals that, in any given iteration, not only,  $\ell_f$ , (may note an earlier related discussion) but also  $q_f$  can be calculated directly based on the current value of  $\Delta$ . However, the  $\ell_f$  and  $q_f$  estimates obtained as such cannot be substituted back into Eqs. 3 and 4 to have an effect on the  $T_a$  and  $\Delta$  values computed in subsequent iterations. Neither the current value of  $\ell_f$  can be substituted into Eq. 2 to have an effect on the estimates of  $q_f$  in subsequent iterations and vice-versa. In other words, evaluation of  $\ell_f$  and  $q_f$  in any given iteration of the alternative models does not contribute to improvements in the solution in subsequent iterations, hence,  $\ell_f$  and  $q_f$  need not be calculated in any of the iterations, except the last.

The preceding analysis conclusively establishes that when model 1, 2, or 3 is used to compute the evaporation variables,  $\ell_f$  and  $q_f$  need to be evaluated only once following

convergence. Also, when coupled with empirical evidence (obtained by way of numerical outputs presented in Tables 3a and 3b), the preceding observations strongly suggest that the mathematical structure of the Penman-Monteith system of equations is such that the iterative solution of the complete set, consisting of Eqs. 1 to 4 (model 4), is unlikely to produce a more accurate solution than the reduced forms (models 1, 2, and 3).

#### **4.7. Comparison of model 1 and the conventional model**

Results of intercomparison of model 1 and the conventional model (i.e., the most widely used formulation) is presented here. Given that both model 1 and the conventional model involve a level of approximation in the computation of  $\Delta$ , direct comparison of the models could not provide answer to the question: which model is more accurate? A more direct way of addressing this question may require comparing both model 1 and the conventional model to a more accurate model. However, such an evaluation is not part of the current study, hence the question of accuracy was not addressed here, directly, as such. Instead, the purpose of model comparison was limited to (i) assessment of the significance of the effects that the different approaches, used by the models to estimate  $\Delta$ , have on variable estimates in general and (ii) highlighting some broader implications of the results on the relative accuracy of the models.

##### **4.7.1. Latent heat flux**

Table 4 presents the variables estimates obtained with model 1 and the conventional model for all the data sets given in Table 1. Note that, for convenience, the data in the outputs section of model 1 (Table 4) simply replicates those presented in Tables 3a and 3b. As can be noted from Table 4, the latent heat flux computed with model 1 varies between a minimum of  $191.3\text{W/m}^2$

(data set 4) and a maximum of  $683.3\text{W/m}^2$  (data set 7). By comparison estimates of  $\ell_f$  obtained with the conventional method range from  $175.1\text{W/m}^2$  (data set 4) to  $654.1\text{W/m}^2$  (data set 7). Furthermore, evaporation flux obtained with model 1 vary between  $6.7\text{mm/day}$  (data set 4) and  $24.1\text{mm/day}$  (data set 7). The conventional approach predicts slightly less evaporation fluxes,  $E_f$ , than that of model 1, which vary between  $6.2\text{mm}$  (data set 4) and  $23.1\text{mm/day}$  (data set 7).

A close look at the data in Table 4 shows that the minimum and maximum of the computed latent heat (or evaporation) flux obtained with both models are observed in data sets 4 and 7, respectively. The low evaporation flux associated with data set 4 can be explained by the fact that data set 4 is characterized by a relatively small external heat flux ( $300\text{W/m}^2$ ), low vapor pressure deficit ( $0.373\text{KPa}$ ), low air temperature ( $278\text{K}$  or  $5^\circ\text{C}$ ), and a relatively large aerodynamic resistance of  $98.4\text{s/m}$ . On the other hand, the external heat flux for data set 7, which is  $400\text{W/m}^2$ , is about 85% of the average across all data sets and the measured air temperature of  $293\text{K}$  is not on the high side. Thus, the likely explanatory factor for the very large latent heat and evaporation fluxes are the very high vapor pressure deficit (of  $2.1\text{KPa}$ ) and to a degree the small aerodynamic resistance of  $28.2\text{s/m}$ . This suggests that in data set 7, the evaporation process was likely dominated by the adiabatic cooling process.

Upon closer examination, the latent heat flux for data set 7 show that the gain in latent heat, in the adiabatic cooling process, expressed in terms of equivalent latent heat flux is  $443.9\text{W/m}^2$ . By comparison, the fraction of the external heat flux, that led to further increases in latent heat content of the air in the diabatic process is  $239.4\text{W/m}^2$ , which is about 53.9% of that associated with the adiabatic component. This observation confirms that the evaporation process in data set 7 was dominated by the adiabatic cooling component, driven mainly by the high vapor pressure deficit and to a degree by the low aerodynamic resistance.

**Table 4.** Comparison of variables estimates computed with model 1 and the conventional model

Variable name	Unit	Model outputs													
		Model 1							Conventional model						
		McArthur's data sets			Additional data sets				McArthur's data sets			Additional data sets			
		Data set 1	Data set 2	Data set 3	Data set 4	Data set 5	Data set 6	Data set 7	Data set 1	Data set 2	Data set 3	Data set 4	Data set 5	Data set 6	Data set 7
Latent heat flux, $\ell_f$	W/m <sup>2</sup>	277.1	373.0	435.6	191.3	339.8	520.5	683.3	201.4	343.7	428.4	175.1	320.2	509.5	654.1
Sensible heat flux, $q_f^{(*)}$	W/m <sup>2</sup>	222.9	127.0	64.4	108.7	80.2	129.5	-283.3	298.6	156.3	71.6	124.9	99.8	140.5	-254.1
Evaporation flux, $E_f^{(*)}$	mm/day	9.8	13.1	15.4	6.7	12.0	18.3	24.1	7.1	12.1	15.1	6.2	11.3	18.0	23.1
Final air temperature, $T_a$	K	291.4	303.5	318.3	286.8	314.5	312.5	286.4	297.7	305.9	318.9	288.2	317.3	312.9	287.1
Saturation vapor pressure related slope parameter, $\Delta$	KPa/K	0.0821	0.1938	0.4465	0.0805	0.3265	0.3478	0.1217	0.0445	0.1452	0.3946	0.0610	0.2442	0.3119	0.1452
Modified psychrometer constant, $\gamma^{(*)}$	KPa/K	-	-	-	0.0697	0.0925	0.1107	0.0816	-	-	-	0.0697	0.0925	0.1107	0.0816
Aerodynamic resistance, $r_a^{(*)}$	s/m	-	-	-	98.4	173.1	42.2	28.2	-	-	-	98.4	173.1	42.2	28.2
Variable name	Unit	-							Summary of residuals between variable estimates obtained with model 1 and the conventional model (%) <sup>(***)</sup>						
									Min		Max			Av	
Latent heat flux, $\ell_f$	W/m <sup>2</sup>	-							1.66		27.32			8.21	
Sensible heat flux, $q_f^{(*)}$	W/m <sup>2</sup>	-							8.53		33.98			18.06	
Evaporation flux, $E_f^{(*)}$	mm/day	-							1.67		27.33			8.21	
Final air temperature, $T_a$	K	-							0.12		2.15			0.69	
Saturation vapor pressure related slope parameter, $\Delta$	KPa/K	-							10.32		45.77			23.07	

<sup>(\*)</sup> Modified psychrometer constant is not given for the McArthur data sets, because it is equal to the psychrometer constant, which was specified at the input (Table 1). The aerodynamic resistance as well is not given at output for McArthur's data sets, because it was specified at the input

<sup>(\*\*)</sup> Min, Max, Av are the minimum, maximum, and average percent absolute residuals, respectively.

<sup>(\*\*\*)</sup> For each variable and data set combination, percent absolute residuals were calculated with:

$$\text{absolute residual} = \frac{|\text{variable estimate with model 1} - \text{variable estimate with the conventional model}|}{\text{variable estimate with model 1}} 100$$

#### 4.7.2. Sensible heat flux

The sensible heat flux computed with model 1 varies between a minimum of  $-283.3\text{W/m}^2$  (data set 7) and a maximum of  $222.9\text{W/m}^2$  (data set 1). On the other hand,  $q_f$  obtained with the conventional model ranges from  $-254.1\text{W/m}^2$  (data set 7) to  $298.6\text{W/m}^2$  (data set 1), Table 4. The maximum residual between estimates of the sensible heat flux, obtained with model 1 and the conventional model, can be appreciable and will be discussed later. However, the point of interest here is physical interpretation of the results, which is presented as follows.

The negative algebraic sign of the minimum sensible heat flux in data set 7 indicates that there was a net decline in the sensible heat content of the air during the evaporation process. However, whether the decrement in the sensible heat content of the air represents not only a net reduction (associated with the adiabatic cooling process that is not fully compensated in the diabatic process), but also a net outflow of heat from the air to the exchange surface, depends on the algebraic sign of the diabatic component of the sensible heat flux.

A close look at the sensible heat flux estimate for data set 7, computed with model 1, reveals that the equivalent sensible heat flux in the adiabatic cooling process is  $-443.9\text{W/m}^2$ . While the negative algebraic sign implies a loss in the sensible heat content of the air in the adiabatic process (at a rate of  $443.9\text{W/m}^2$ ), it can, nonetheless, be deduced based the analysis in Chapter 2 that the loss was not because of a transfer of heat from the air to the exchange surface. Instead, it was due to the conversion of sensible heat to an equivalent amount of latent heat, as a result of which the total heat content of the air remained constant.

In the diabatic process, on the other hand, the sensible heat fraction (of the external heat flux) is  $160.6\text{W/m}^2$ . The positive algebraic sign of the sensible heat flux associated with the diabatic component shows that it represents a transfer of heat from the exchange surface to the

air and hence an increase in the sensible heat content of the air. Note that this observation could have also been deduced from the algebraic sign of the external heat flux for data set 7, which is  $400\text{W/m}^2$ , and alternatively from the algebraic sign of the latent heat flux associated with the diabatic process, which is  $239.4\text{W/m}^2$ .

The preceding shows that the negative algebraic sign of the net sensible heat flux for the entire evaporation process ( $-283.3\text{W/m}^2$ , Table 4), which is equal to the algebraic sum of the adiabatic and diabatic components of the sensible heat flux, is not caused by a net transfer of heat from the air to the exchange surface. Instead, it is attributable to the imbalance between the decrement in the sensible heat content of the air that occurred (at a steady rate of  $-443.9\text{W/m}^2$ ) in the adiabatic process, through conversion to latent heat, and the increment that occurred in the diabatic process (at a rate of  $160.6\text{W/m}^2$ ), which led to a net overall negative sensible heat flux.

Notably, the preceding discussion shows that the thermodynamic conceptualization of evaporation does not just allow for the quantification of the latent heat and sensible heat fluxes, but also reveals more readily the physical processes that derive changes in the heat contents of the air and the modes of interaction of the ambient air with the source/sink surface during an evaporation process.

#### **4.7.3. Final (equilibrium) air temperature and slope parameter related to the saturation vapor pressure function**

As can be noted from Table 4, estimates of the final air temperature obtained with model 1 vary between a minimum of  $286.4\text{K}$  (data set 7) and a maximum of  $318.3\text{K}$  (data set 3). The surface temperature (which is equivalent to the final air temperature in model 1) calculated with the conventional model ranges between  $287.1$  (data set 7) and  $318.9\text{K}$  (data set 3). Furthermore, estimates of  $\Delta$  obtained with model 1 ranges from  $0.0805$  (data set 4) to  $0.4465\text{KPa/K}$  (data set

3). By comparison, the  $\Delta$  value calculated with the conventional model vary between 0.0445 (data set 1) and 0.3946 KPa/K (data set 3).

#### **4.7.4. Percent absolute residuals between variable estimates obtained with model 1 and the conventional model**

A summary of the overall percent absolute residuals between the variable estimates obtained with model 1 and those of the conventional model is presented in the residuals section of Table 4. In addition, however, the minimum, maximum, and average percent absolute residuals between variable estimates computed with model 1 and those obtained with the conventional model are depicted in a grouped bar chart (Figure 3). As can be noted from Figure 3 and Table 4, with a maximum percent absolute residual of about 45.8% and a mean residual of 23.1%, the largest residual between the variables computed with the conventional model and model 1 is associated with estimates of  $\Delta$ .

By comparison, the smallest percent absolute residual is observed for the final air temperature, with a maximum value of about 2.2% and a mean of 0.7%. The results also show that the variable most affected by the difference in the approaches used to estimate  $\Delta$ , in the models, is the sensible heat flux, which has a maximum residual of about 34.0% and an average value of 18.1%. Although the rather more important parameters of latent heat flux and evaporation flux have a relatively large maximum residual of about 27.3%, the average residual for both parameters is a much smaller amount of 8.2% (Table 4). These results suggest that differences in the methods used for estimating  $\Delta$  have the maximum effect on sensible heat flux estimates, a negligible effect on estimates of  $T_a$ , and a limited effect on the estimates of latent heat and evaporation fluxes.

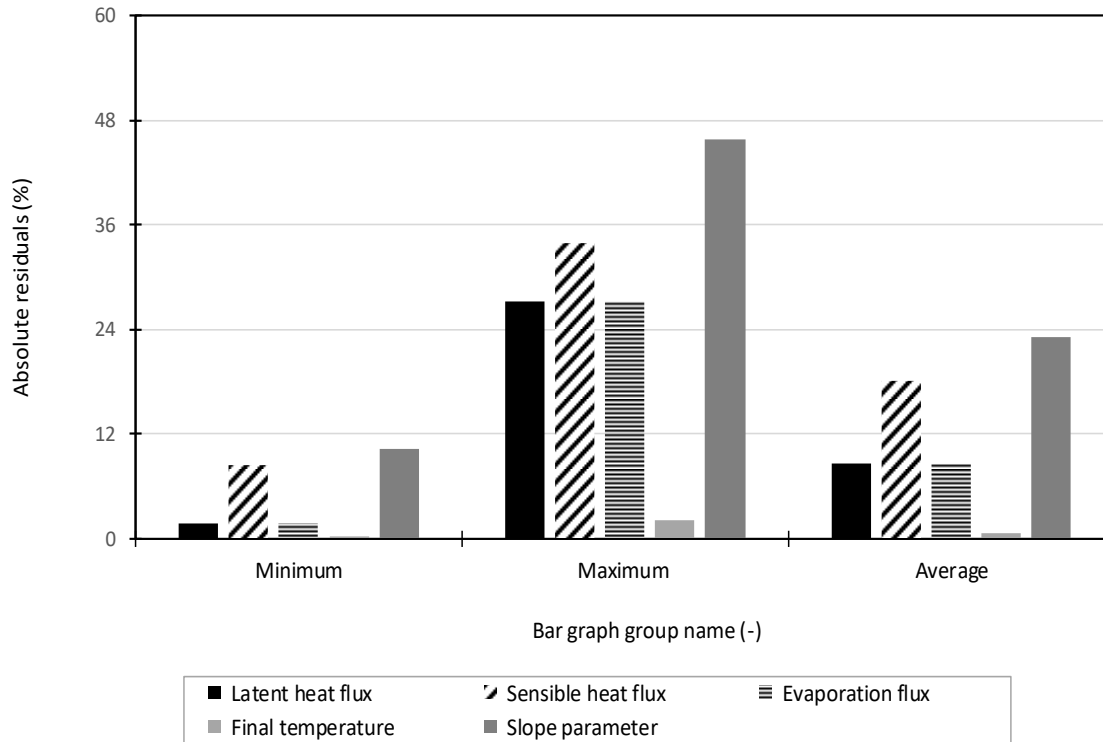


Figure 3. Absolute residuals between variable estimates computed with model 1 and the conventional model (All data sets, Table 1)

It is important to note here that both model 1 and the conventional model are based on simplifying assumptions and hence outputs of both models involve a level of approximation. The implication is that the accuracy of the conventional model and model 1 cannot be evaluated through direct intercomparison of the models. Such an assessment, instead, requires the variable estimates obtained with each model (i.e., the conventional model and model 1) to be compared with those of a more accurate model (likely a mechanistic simulation model) of evaporation from a cropped field, that couples vapor, heat, and momentum transfer and transport processes through the soil-crop-atmosphere continuum, taking into account wind induced advection and forced convection. Thus, evaluation of the accuracy of the proposed model (model 1) relative to that of the conventional approach is not the objective of the study reported here. However, considering

evaporation flux (i.e., the single most important variable in so far as agricultural water management is concerned), the relatively large maximum percent absolute residual of 27.3% suggests that potentially there can be significant differences between the evaporation flux estimates of the two methods.

Generally, the average residual, instead of the maximum, is more representative of the difference between variable estimates computed with model 1 and the conventional model. Thus, the relatively small mean absolute residual (of 8.2%) for  $\ell_f$  suggests that differences in  $\ell_f$  estimates computed with model 1 and the conventional model should typically be within the margin of error of the conventional model. This result points to the fact that, from the standpoint of accuracy, both models may, on average, represent equally adequate description of natural evaporation

## **Chapter 5. Summary and conclusion**

In this report, the Penman-Monteith equation is derived based on the thermodynamic conceptualization of evaporation proposed by Monteith. It is shown that the derivation leads to a set of equations (consisting of expressions for latent heat flux, sensible heat flux, and the final air temperature) that represent a coupled system. The report detailed the development and evaluation of alternative numerical solutions to the coupled set of equations. Furthermore, relationships between resistance parameters used to define the Penman-Monteith system of equations are explored and equations used to evaluate them are reviewed.

A review of Monteith's thermodynamic approach to the derivation of the Penman-Monteith equation is presented in Chapter 2. While essentially reviewing the work of Monteith, the study

presented here emphasizes basic assumptions that the derivation is based on, clarifies concepts, and fills gaps left in the original discussion. In addition, it focusses on mathematical/physical interpretations of the terms and key parameters of the equation.

Unlike the conventional approach to the derivation of the Penman-Monteith equation, where evaporation is treated as vapor and heat transfer process between two points in space (i.e., a point in the exchange surface and another one in the air current), the thermodynamic conceptualization of evaporation introduces a perspective whereby evaporation is viewed from the vantage point of the changes it produces in the thermodynamic properties of the air. Accordingly, the derivation of the Penman-Monteith equation presented here describes evaporation as a physical process consisting of a pair of formal thermodynamic subprocesses (comprising, adiabatic cooling and diabatic heating) that leads to an increase/a decrease in the energy states of the ambient air in a way that is readily quantifiable.

The Penman-Monteith equation is derived in two steps. As an initial approximation, a form of the equation that models evaporation from a wet surface into a stationary ambient air is developed based on the thermodynamic equations of state applied to a suitably defined system. Resistance parameters are then introduced into the basic equations, in a subsequent step, accounting for the dynamic effects of wind-surface interaction [and the (bulk) canopy system response to atmospheric conditions] on evaporation, leading to the Penman-Monteith equation.

Although less compact than the conventional approach, the thermodynamic approach to the derivation of the Penman-Monteith equation has the benefit of revealing key assumptions and concepts that are generally implicit in the conventional approach. Important observations stemming from the thermodynamic based derivation of the Penman-Monteith equation are summarized here:

(1) The method accentuates the notion that the Penman–Monteith equation is fundamentally a description of the process of vapor and heat transfer between a wet source/sink surface and a quiescent ambient air (the first step of the derivation with the thermodynamic approach).

(2) It also underlines the fact that the effects, of crop-canopy complex response to atmospheric conditions and convective transport, on heat and vapor transfer are taken into account in an approximate sense through the introduction of resistance parameters to the basic equations of state (the second step of the derivation with the thermodynamic approach).

(3) The thermodynamic approach also shows that evaporation is a process essentially driven by energy (heat) supply and as such, each term of the Penman–Monteith equation represents a separate heat source for evaporation, consisting of an external heat flux from the surface for the diabatic process and sensible heat extant in the air at the start of evaporation for the adiabatic process.

(4) Given that the thermodynamic approach is based on conceptual charts depicting the energy states of a suitably defined thermodynamic system, it readily reveals the mathematical attributes of a key parameter of the Penman–Monteith equation, namely the slope parameter related to the saturation vapor pressure curve,  $\Delta$ .

(5) Notably, a close look at the charts shows that evaporation can occur with a surface temperature that is less than the air temperature, provided the surface temperature is greater than the dewpoint temperature. and

(6) The results also suggest that the thermodynamic description of the terms of the Penman–Monteith equation as adiabatic and diabatic components might be a more precise interpretation of the physical meaning of the terms.

The derivation presented in Chapter 2 produces equations for computing the latent heat flux, sensible heat flux, and the final air temperature under conditions of natural evaporation. The equations are expressed as functions of the bulk surface resistance and the resistances to vapor and heat transport across the turbulent boundary layer. Under a suitably defined atmospheric condition, the aerodynamic resistance to vapor transfer is shown to be the same as that of heat transfer, leading to a simplification of the modified psychrometer constant and hence to the common form of the Penman-Monteith equations.

Another important physical process integral to evaporation and inextricably coupled to the convective transport of vapor and heat is that of momentum transfer. Chapter 3 derives an equation for the aerodynamic resistance to momentum transfer and presents a relationship between the resistance parameters to the convective transfer of momentum and that of vapor/heat. The chapter then closes with a description of the equation widely used to estimate the aerodynamic resistance to vapor/heat transfer and a reference to a method used for estimating the bulk surface resistance in agricultural water management applications.

The system of equations derived in Chapter 2 constitutes a coupled set. Description of numerical solutions for the Penman-Monteith system of equations is presented in Chapter 4. Alternative numerical solutions ranging in complexity from those involving the solution of a subset of the system of equations to one solving a form of the complete set are developed and evaluated here.

Accordingly, four alternative algorithms, referred to as model 1, 2, 3, and 4, are presented. Models 1, 2, and 3 use a two-step approach to determine the variables:  $\ell_f$ ,  $q_f$ ,  $T_a$ . Model 4, on the other hand, computes latent heat,  $\ell_f$ , sensible heat,  $q_f$ , and final air temperature,  $T_a$ , through a simultaneous iterative solution of the complete set.

Results of model verification showed that each of the alternative models produced outputs essentially identical and also in close agreement with a reference solution. The average absolute residuals between the predictions of the models presented here and those of the reference solution vary between about 0.2% observed for  $T_a$  and a maximum of 1.9% for  $\Delta$ . In addition, comparison of the alternative models based on the criteria of numerical efficiency and robustness suggests that each model represents a comparable alternative, to any of the other models, for estimating evaporation. However, owing to its simplicity, model 1 is considered for further analysis.

The models developed in the current study compute  $\Delta$  as part of the solution. A more widely used approach described here as the conventional model, on the other hand, determines  $\Delta$  independently (by setting it equal to the slope of the saturation vapor pressure curve at the measured air temperature), leading to an uncoupled system of equations that can be solved directly.

A comparison of the outputs of the conventional model with those of model 1 was conducted, in the current study, based on a total of seven hypothetical data sets, covering a wide range of natural evaporation conditions. The results suggest that differences in the methods used for estimating  $\Delta$  have the maximum effect on sensible heat flux estimates (where the mean absolute residual is 18.1%), a negligible effect on estimates of final air temperature (with an

average residual of 0.7%), and a limited effect on the estimates of latent heat and evaporation fluxes, in which the mean residual is 8.2%.

Both model 1 and the conventional model involve a level of approximation in the determination of  $\Delta$ , thus, a direct comparison of the two models cannot provide an answer to the question: which model is more accurate? In other words, the current study does not address the question of accuracy. However, the fact that the average residual for  $\ell_f$ , over all the data sets is only 8.2%, suggests that differences in  $\ell_f$  estimates computed with model 1 and the conventional model, should typically be within the margin of error of the conventional model (the more widely used of the two models compared here). This observation suggests that from an agricultural water management perspective, both the conventional model and model 1 can, on the average, be considered equally valid descriptions of natural evaporation.

A cautionary note is, nonetheless, in order here. Although the data used in the analysis cover a range of evaporation scenarios, they are limited and hence a conclusive deduction on this may need to await a more comprehensive follow up study focused on a comparative evaluation of model 1 and the conventional model.

## References

- Allen, R. G., Pereira, L.S., Raes, D., Smith, M. (1998). “*Crop evaporation, Guidelines for Computing Crop Water Requirements*” FAO Irrigation and Drainage Paper 56. UN Food and Agriculture Organization, Rome.
- Arya, S.P. (1991). “*Introduction to Micrometeorology*” Academic Press, Inc, New York, NY.
- Bristow, K.L. (1987). “On Solving the Surface Energy Balance Equation for Surface Temperature.” *Agric. For. Meteorol.*, 39:49-54.

- Brutseart, W. (1982). “*Evaporation into the Atmosphere, Theory, History, and Applications*”  
D. Reidel Publishing Company, Dordrecht, The Netherlands.
- Doorenbos, J. and Pruitt, W.O. (1977). “*Guidelines for Predicting Crop Water Requirements*”  
FAO Irrigation and Drainage paper No. 24. Second ed. UN Food and Agriculture  
Organization, Rome.
- Howell, T.A., and Evett, S.R. (2004). “The Penman-Monteith Method. Section 3 in  
Evapotranspiration: Determination of Consumptive Use in Water Rights Proceedings.”  
*Continuing Legal Education in Colorado*, Inc. Denver, CO.
- Jensen, M.E. and Allen, R.G. (2016). “*Evaporation, Transpiration, and Irrigation Water  
Requirements*” Second ed., ASCE Manuals and reports on Engineering Practice No. 70.  
ASCE.
- Lascano, R.J. and van Bevel, C.H.M. (2007). “Explicit and Recursive Calculation of Potential  
and Actual Evapotranspiration.” *Agron. J.* 99:585-590.
- McArthur, A.J. (1990). An accurate solution to the Penman equation. *Agricultural and Forest  
Meteorology*, 51(1990):87-92.
- McArthur, A.J. (1992). “The Penman Form Equations and the Value of Delta: A Small  
Difference of Opinion or A Matter of Fact?” *Agric. For. Meteorol.*, 57(1992): 305-308.
- Monteith, J.L. (1965). Evaporation and Environment. *Symposia of the Society for Experimental  
Biology*. 19, 205-234.
- Monteith, J.L. (1981). Evaporation and surface temperature. *Quarterly Journal of the Royal  
Meteorological Society*. 107, 1-27.
- Monteith, J.L. and Unsworth, M.H. (2013). “*Principles of Environmental Physics, Plants,  
Animals, and Atmosphere*” Fourth ed., Elsevier.

- Paw, U.K.T. and Gao, W. (1988). Applications of Solutions to Non-Linear Energy Budget Equations. *Agric. For. Meteorol*, 43(1988): 121-145.
- Penman, H.L. (1948). Natural evaporation from open water, bare soil, and grass. Proceedings of the Royal Society of London , A 194, 120-145.
- Penman, H.L. (1953). "The Physical Basis of Irrigation Control." *Rep. 13<sup>th</sup> Int. Hort. Cong. 2*, 913-923.
- Penman, H.L. and Long, I.F. (1960) Weather in wheat: As essay in micro-meteorology. *Quart. J. R. Met. Soc.* 86:16-50.
- Rajput, R.K. (2007). *Engineering Thermodynamics*. Third ed. Laxmi Publications, Ltd. Boston.
- Thornthwaite, C.W. and Holzman, B. (1942). "*Measurements of Evaporation from Land and Water Surface*" US Department of Agriculture Technical Bulletin, vol 817, US Department of Agriculture, Washington, DC, pp. 75.
- Watkins, D. S. (2010). *Fundamentals of matrix computation*. 3rd ed. New York: Wiley.